Carbonates and Evaporites (2022) 37:62
https://doi.org/10.1007/s13146-022-00802-4

ORIGINAL ARTICLE

Geochemical evolution of structure-bedding controlled hydrothermal dolomites of the Kinta Valley, Western Malaysia

P. Xin Hui[1] · R. Nagarajan[2,3] · Mu. Ramkumar[4,5] · T. F. Ng[6] · Nur I. Taib[6] · M. J. Mathew[7] · B. Sautter[8] · N. A. Siddiqui[1] · M. C. Poppelreiter[5]

Accepted: 15 August 2022 / Published online: 30 August 2022
© The Author(s) 2022

Abstract

Study of secondary dolomitization and documentation of the evolution of basinal fluids and host rock, especially that of fine-grained deepwater carbonate mudstone are of interest toward of reservoir characterization. From this perspective, field characteristics in relation to mineralogy, petrography and geochemistry of the Paleaozoic carbonates of the Kinta Valley, Peninsular Malaysia, were investigated and documented. A total of 33 samples were collected across the various degree of dolomitization and analyzed for their petrographic properties ($n = 55$), while mineralogical and geochemical compositions ($n = 33$) were analyzed using XRD, ICP and ICPMS analysis, respectively. These analyses were performed to elucidate the diagenetic events, episodic dolomitization and development of fluid evolution as a function of regional tectono-thermal events during the Permian to Cenozoic. It is interpreted that the host calcareous mudstones (HCMs) were deposited in oxygenated, open marine seawaters. The studied samples retain the original seawater characteristics despite negligible, minor alterations of REE characteristics due to diagenesis and detrital input. Though the concentrations and trends of REEs of the dolomitic facies are modified to a certain extent, their affinities with HCMs are preserved. Enrichments of Mg, Mn, Na and depletion of Sr are linked to the effect of dolomitization under the open system of diagenesis. The redox conditions fluctuated to show distinct, recognizable variations between different dolomite phases. The MREE enrichments with other trace elements such as Mn, Fe and low Sr content indicate the association of diagenetic fluids with deep-circulating crustal hydrothermal fluids. Hydrothermal influence has been recorded along the fractures, which might have originated from the sub-surface litho units and facilitated episodic dolomitization, especially during significant tectono-thermal events. This study affirms that the occurrence, geochemical and mineralogical evolution of the dolomites of the Kinta Valley were controlled by magmatic events, whereas the intensity of replacement dolomitization was controlled by host rock texture, varied bulk chemistry of host rock, circulating fluid and temperature.

Keywords Calcareous mudstone · Diagenesis · Dolomites · Geochemistry · Hydrothermal diagenetic fluids

Introduction

Nearly half of the Earth's carbonate rocks are dolomitized (Zenger et al. 1980; Warren 2000; Machel 2004; Escorcia et al. 2013). Approximately 60% of oil and 40% of gas reserves occur in the carbonates of the World and among which, substantial hydrocarbon reservoirs are found in dolomitized carbonates (Purser et al. 1994; Braithwaite et al. 2004; MacDonald et al. 2015). Hence, sedimentologists and petroleum geologists are working on improving the current understanding of the origin and documentation of occurrences of dolomites (Machel 2004; Anan and Wanas 2015; Saleem et al. 2022). These endeavors bear scientific significance and economic value as potential hosts for hydrocarbon reserves (Martín-Martín et al. 2015). Accurate characterization of carbonate reservoirs requires systematic documentation of prevalent diagenetic processes as the rock fabrics are significantly modified and porosity increased/altered during diagenesis (Vandeginste et al. 2013). Dolomitization is one of the key diagenetic processes that control carbonate reservoir quality and heterogeneity (Zenger et al. 1980; Sun 1995; Braithwaite et al. 2004; Wilson et al. 2007). It can strongly impact the petrophysical properties of the carbonate rocks (Vandeginste et al. 2013) by modifying original

✉ R. Nagarajan
nagarajan@curtin.edu.my

Extended author information available on the last page of the article

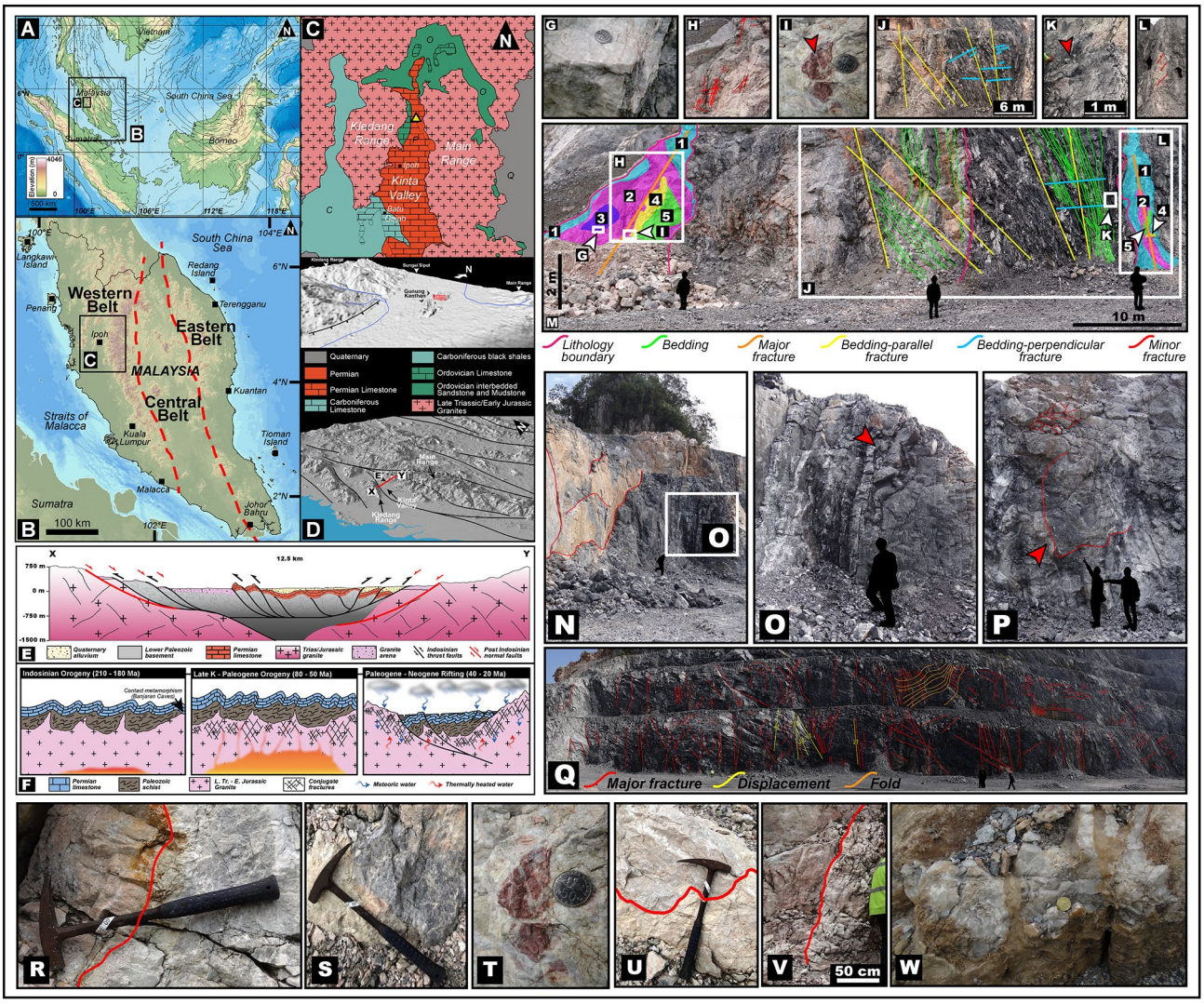

depositional textures, porosity and permeability distribution (Chen et al. 2004). These changes in turn influence fluid flow and oil recovery (Warren 2000). The distribution of rock heterogeneities that resulted from the evolution of basinal fluids, fluid–rock interactions and mineralization govern the occurrences of dolomitized bodies in the subsurface. Nevertheless, their relationships and the extent of influence on reservoir quality are still poorly constrained (e.g. Sun 1995; Duggan et al. 2001; Chen et al. 2004; Ronchi et al. 2012a; Vandeginste et al. 2013; Martín-Martín et al. 2015).

Application of major, trace and rare earth elements (REE) as geochemical proxies is gaining wide acceptance in carbonate provenance studies and the environmental settings during carbonate deposition/precipitation (Banner et al. 1988a, b; Kamber and Webb. 2001; Nothdurft et al. 2004; Frimmel 2009; Nagarajan et al. 2011; Azomani et al. 2013; Zhao and Jones 2013; Zhao and Zheng 2014; Li et al. 2017; Srivastava and Singh 2019; Guruaribam et al. 2021) and post-depositional alteration (Delpomdor et al. 2013; Nagarajan et al. 2013; Wang et al. 2014; Franchi et al. 2015; Ganai et al. 2018; Dutt et al. 2021). This paper presents petrographic, mineralogical and geochemical data, regarding which discussion on the occurrences of polyphase dolomite geobodies, examination of the strata and structural controls are attempted. These were utilized to interpret hydrothermal dolomites' genetic and paragenetic sequences and to demonstrate how the regional tectonic evolution affected paragenesis.

Regional geological setting

Peninsular Malaysia (Fig. 1A) lies on the western part of the Sundaland and can be structurally and geologically divided into the following three north–south trending regions (Fig. 1B): the Western, the Central and the Eastern belts (Lee 2009; Metcalfe 2013). The Western and Central belts lie on the Sibumasu terrane, while the Eastern Belt is part of the East Malaya block (Metcalfe

◂**Fig. 1** **A–D** Regional geological setting, structural trends and location of the study area (modified after Ramkumar et al. 2019). **A** Simplified regional topographic map showing the regional setting and location of the Kinta Valley in western Malaysia. **C** Geological map showing sprawl of Kinta Valley, geology of the region and location of the study area, sandwiched between two granitic plutons. **D** Digital Elevation Model (DEM) of the region manifesting landscape and regional structural trends of the Kinta Valley and adjoining regions. **E–F** Major tectono-magmatic events in and around Kinta Valley in the western belt, Western Malaysia. **E** Cross section across the profile indicated in **D**; **F** Sketches of tectono-magmatic events, successive stages and resultant structural deformations. **G–M** LaFarge quarry face exposes strata-bound and fault-related dolomite phases and host calcareous mudstone (HCMs), and well-preserved structural characteristics. **G** Millimeter-thick, multi-directional veins cut through all the facies types, representing the last generation of fractures. **H** Second set of thinner and irregularly oriented fractures. **I** Brecciated HCM and dolostone found at the foot of the fracture. **J** First set of fractures characterized by bedding parallel, tangent and perpendicular NW–SE and E-W oriented dolomite-filled fractures cutting through the HCM. **K** Slickensides in the fracture-controlled dolostone reflecting brittle deformation. **L** NW–SE oriented dolomite-filled fractures exposed on the smaller inverted "V" fracture in the mine wall. **M** Lafarge quarry face exposing strata-bound and fault-related dolomite phases and HCMs, each with a distinct texture, form, geometry, morphology and associated fracture patterns and orientations. **N–Q**. Field-scale structures and fracture patterns on the quarry wall opposite the wall are depicted in **M**. **N** Evidences of fluid movement and brittle deformations such as thin-bedding parallel fractures and slickensides as explicit in a distinct coloration. The occurrence of this bedding parallel fracture is observed on the opposite mine wall located away from the fracture shown in **M**. Continuation of the fracture shown in **M** is traceable through the mine floor to this location. The red box area shows ductile deformation characterized by folding. **O** Close-up view of the ductile deformation shown in the previous photo. Boudins (?) indicated by the red arrow are visible as manifested by the thickening and thinning of beds and folding. **P** Brittle deformations are observed on another section of this same mine wall, characterized by thin fractures (indicated by red lines) and breccia (indicated by red arrow). **Q** Structural characteristics are characterized by fractures (indicated by red lines), displacements (indicated by yellow lines) and folds (indicated by orange lines). **R–W**. Dolomite and calcite facies types. **R** Early replacement dolomite (P2). Dolomites (P2) and HCMs (P1) are easily distinguished by the color differences between yellowish orange (dolomites) and light to dark grey color (HCM). The contact between HCMs (P1) and dolomite (P2) is gradual. **S** Sucrosic dolomite (P3) exhibits a sugary texture, associated with multi-directional criss-cross fractures and kinks. **T** Sharp contact between metamorphosed dolomite (P4) and early replacement dolomite (F2), and minor fractures filled with calcite veins. **U** Late replacement dolomite (P5) is characterized by its white color appearance associated with dense fractures. **V** Brecciated HCM (P1) and early replacement dolomite (P2). Angular clasts of breccia fragments are cemented by white-colored calcite. **W** Perfectly developed, transparent rhombohedral calcite crystals of the last phase of the diagenetic history

2013). The former consists of the Main Range plutons and the latter consists of the Eastern Malaya plutons (Searle et al. 2012). The collision between Sibumasu and East Malaya in the Early to Middle Triassic is evidenced by the Bentong–Raub Suture (Harbury et al. 1990; Metcalfe 1991; Hutchison 1994) which marks the closure of the Paleo-Tethys (Hutchison 1994; Metcalfe 2011a; Searle et al. 2012; Cottam et al. 2013).

From being part of Indochina and Cathaysia, the East Malaya Block was separated from the Gondwana during the Early Paleaozoic as a result of the opening of the Paleo-Tethys (Metcalfe 2011a). Based on faunal and floral evidences, the Cathaysia block was interpreted to have experienced warm-water equatorial climate since the Carboniferous (Metcalfe 2011a). On the contrary, Sibumasu was characterized by cold-water biotas displaying the Gondwana affinity until the Permian (Metcalfe 2011a). Later, it was detached from the Gondwana, concomitant with the opening of the Meso-Tethys (Wakita and Metcalfe 2005). The occurrence of subduction-related Latest Permian to Triassic calc-alkaline magmatism on both the blocks was linked to the convergence of the two blocks (Searle et al. 2012). Following this period of subduction, the intra-oceanic Sukhothai Arc separated from the East Malaya, and the two blocks collided prior to the arrival and docking of the Sibumasu (Metcalfe 2011a) with the East Malaya and the Sukhothai Arcs. This collision resulted in a sequence of events such as crustal thickening, regional metamorphism (Searle et al. 2012) and emplacement of the Late Triassic S-type granitoids in the Western Belt (Krähenbuhl 1991; Searle et al. 2012; Ghani et al. 2013; Ng et al. 2015a, b). The eminent late-orogenic acidic granitic intrusions, distinguished by melting of the deep crust (anatexis), testify to the intensity of this thermal event (Metcalfe 2013; Sautter et al. 2017). During the Late Cretaceous, magmatism was significant in the Eastern Belt (Searle et al. 2012). An anomalous thermal history across the Malay Peninsula region during the Late Cretaceous is evidenced by the emplacement of several isolated plutons (Ghani et al. 2013; Ng et al. 2015a, b; Md Ali et al. 2016). Throughout the late Early Cretaceous to the Early Cenozoic, the Main Range granites in the Western Belt underwent high-intensity fracturing while sedimentary units were folded extensively. It was then accompanied by the exhumation of the granitic bodies (Krähenbuhl 1991; Cottam et al. 2013; Md Ali et al. 2016; François et al. 2017; Sautter et al. 2017). The underlying mechanisms of the series of events are still poorly understood, although cessation of subduction along the Sunda margin and subsequent collision of various microcontinental fragments with the southern margin of Sundaland (Clements et al. 2011; Hall 2012; Cottam et al. 2013) are presumed and await affirmative documentation. An early extension movement stretching N–S in the Latest Cretaceous to the Early Paleocene was reported (Kawakami et al. 2014; Md Ali et al. 2016; François et al. 2017; Sautter et al. 2017, 2019). Rapid exhumation of the plutons during the Late Eocene to the Oligocene was interpreted to have counteracted the resumption of the subduction event with extensional detachments located all around the Sunda margin (Cottam et al. 2013) at nearly 45 Ma (Hall 2012).

The Kinta Valley (Fig. 1B and C) is located in the central part of the Western Belt. This is a V-shaped valley with limestone hills located between northeast–southwest trending Kledang Range in the west and the Main Range Batholith in the east (Fig. 1C and D). Despite being studied for one and a half-century (e.g. Rastall 1927; Jones 1970; Lee 2009), for tin deposits, the regional lithostratigraphy, chronostratigraphy, depositional environments and thermal history and resultant changes in the rocks are yet to be systematically documented/understood. The Paleaozoic Kinta Limestone deposited during the Silurian to the Permian (Hassan et al. 2014), is a 700-m limestone succession, extending across the western belt of Peninsular Malaysia (Fontaine and Ibrahim 1995; Lee 2009; Metcalfe 2011b).

The carbonates of the Kinta Valley were largely affected by two intensive thermo-tectonic events (Metcalfe 2013): first, the intrusion of the S-type granitic plutons during the Late Triassic to the Early Jurassic (Rastall 1927; Lee 2009; Metcalfe 2013) and second, during the Middle to the Late Cretaceous where significant folding and faulting (Harbury et al. 1990; Krähenbuhl 1991; Shuib 2009) affected the Main Range granites of the Western Belt (Harun 2002). This was associated with the emplacement of isolated granitic plutons (Searle et al. 2012; Cottam et al. 2013; Ng et al. 2015a, b). This poorly explained Late Cretaceous diffuse orogenic event is also caused by the clogging of the Upper Cretaceous faults and pluton edges by immense amounts of acidic/felsic fluids (Sautter et al. 2017). These dykes are dated through associated chronological events, along with evident rigorous hydrothermal circulation regionally during the Late Mesozoic and pre-date the regional extension in the Cenozoic. It is herein inferred that the extensive recrystallization and dolomitization affecting the Kinta host calcareous mudstones (HCMs) were also the result of these thermal events (Fontaine and Ibrahim 1995; Lee 2009). The chronological sequence of these major tectono-magmatic events and subsequent structural deformations (Ramkumar et al. 2019) are presented in Fig. 1E and F.

Materials and methods

Initially, documentation of structural settings through regional mapping was attempted with the help of SRTM (Shuttle Radar Topography Mission) 30 m Digital Elevation Models (SRTM data of 30 m resolution available at NASA website) of the Peninsular Malaysia (Fig. 1D), published literature and data on regional geology and structural trends (Fig. 1B–D). It was followed by a field study to select suitable outcrops and quarry sections (LaFarge Quarry – Fig. 1G–Q) in the Kinta Limestone of the Kinta Valley and to document structural data and tectonic structures (Fig. 1M–Q), facies characteristics at the field (Fig. 1R–W), and occurrence and compositional phases of dolomites (Fig. 1R–W). The dolomites were characterized through structural and textural characteristics, various lithofacies types, contact relationships with other lithofacies, dolomite phases, etc. (Fig. 1G–Q). A total of 33 samples including 20 core samples were obtained from various facies types including the HCM, strata-bound, and fracture-controlled dolomites and dolocalcites, dolomite phases and other facies types across the HCM and fracture-fills (dolomite, dolocalcite, calcite and marble) for further analyses. A total of 55 thin sections were prepared from these samples and were first subjected to staining techniques by using a mixture of Alizarin Red-S and potassium ferricyanide for distinguishing calcite from dolomite and ferroan carbonate from non-ferroan carbonates (Dickson 1965; Adams et al. 1984). Detailed petrographic analysis was carried out using the laboratory's reflected and transmitted light microscopes to categorize the textural and morphological types for each carbonate phase recognized in the field (Fig. 2A–L). Petrographic characteristics including crystal morphology, size, textures, dolomite sizes and textures, and relationships with matrix, clasts and other cements were examined. Petrographic classifications of dolomites proposed by Folk (1974) and Sibley and Gregg (1987) were employed for descriptions of the dolomite sizes and textures, respectively. Other detailed petrographic features such as the occurrence of stylolites, recrystallization, zoning, corrosion, overgrowth, dissolution–precipitation, and dissolution-replacement and their cross-cutting relationships were also documented if any.

All the samples ($n = 33$) were ground into powder of 63 µm size using agate mortar and pestle to ensure homogenization of the sample, minimize the effects of varied particle sizes for clay mineralogy, and complete digestion for analyses of whole-rock geochemistry. Mineralogical analyses were performed using an Empyrean diffractometer, PANalytical in the University of Malaya. The finely powdered samples were packed into the sample holder for X-ray diffraction analysis. Patterns were recorded in the range of 2θ from 5 to 90 degrees at 45 kV and 40 mA using Cu radiation, with a step size of 0.026° and 150 s per step. A quantitative analysis was conducted using phase analysis software (HighScore Plus Software version 3.0d), adopting the Rietveld method. Whole-rock geochemical analysis was carried out in the Activation Laboratories Ltd, Canada using Code 4LITHO (11+) Major Elements Fusion ICP(WRA)/Trace Elements Fusion ICP/MS(WRA4B2) package. A known weight of the sample was fused with lithium metaborate/tetraborate in platinum crucibles and the molten sample was cast into a glass disc and the analysis was carried by XRF for major oxides. For the trace and REE analysis, the molten bead was digested rapidly with a weak nitric acid solution. The fusion ensured the dissolution of the entire sample and the analysis was carried out by ICP and ICPMS. Certified

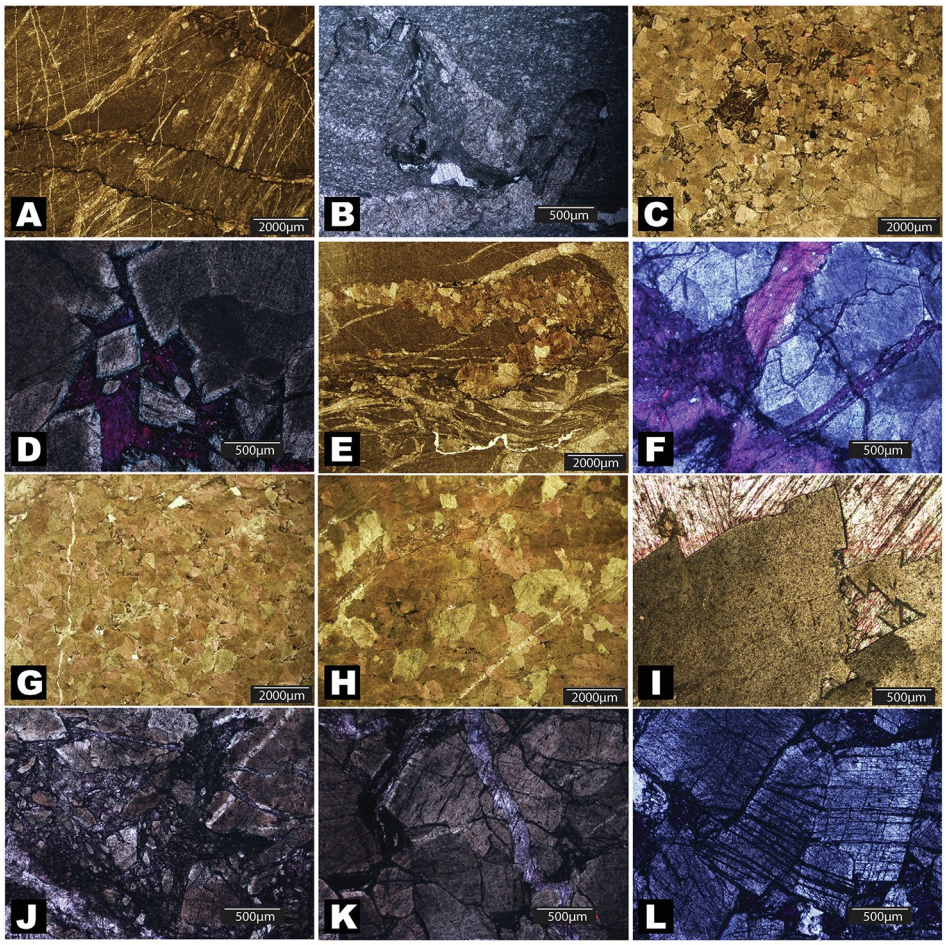

Fig. 2 Photomicrographs showing textural characteristics and relationships of the various facies types found in the quarry wall (all microphotographs are taken under polarized light. the Scale bar is in the photograph itself). **A** Association of low amplitude stylolites in HCMs (P1) reflects compaction in the host rock which resulted in dewatering of HCMs and evolved into dolomitizing fluids together with Mg ions. **B** Occurrence of tectonic stylolites in HCMs (P1) indicates occasions of tectonic compression, testifies the happenings of tectonic events. **C** Microscopic texture of early replacement dolomites (P2) showing 100–1000 µm sized planar euhedral to subhedral dolomite crystals with idiotopic to hypidiotopic mosaics and non-planar anhedral dolomite crystals with xenotopic mosaic are 100–2000 µm sized. P2 dolomite facies exhibit majority of idiotopic mosaic and relatively smaller grain sizes. P2 dolomites indicates replacement with the presence of precursor limestone relicts. **D** Few of the planar euhedral dolomite crystals of early replacement dolomites (P2) have a cloudy core with a clear rim. **E** Formation of early replacement dolomites (P2) along stylolites may indicate a localized source of Mg ions for dolomite cementation. **F** Association of early replacement dolomites (P2) with calcite veins of varied compositions as evident in different colors in stained calcite veins. **G** Microscopic texture of sucrosic dolomites (P3) showing coarse to very coarse (200–2000 µm) planar-s to non-planar-a with hypidiotopic to xenotopic mosaics and medium to coarse (100–400 µm) planar-e dolomite crystals with idiotopic mosaics. P3 dolomite crystals show majority of hypidiotopic texture and relatively larger grain size that that of P2 dolomites, testifying higher degree of recrystallization. The presence of HCMs' relicts again implies replacement. **H** Microscopic texture of late replacement dolomite (P5) exhibits coarse to very coarse (1000–2000 µm) planar-e and –s to non-planar-a dolomite crystals with idiotopic to hypidiotopic and xenotopic mosaics. P5 dolomite crystals exhibit tightly interlocking xenotopic mosaic, with relatively largest grain sizes implying highest degree of recrystallization. Relicts of precursor limestone are also present but in a relative smaller amount reflecting relatively less replacement. **I** Occurrence of saddle dolomites in late replacement dolomite facies (P5) characterized by large crystal size (coarse to very coarse), curved crystal faces, and scimitar-like terminations pointing to pore spaces. **J** Microscopic view of brecciated HCM and dolostone (P6) showing planar subhedral dolomite crystals of various sizes, ranging from 50–500 µm. **K** The brecciated dolomites in P6 facies are cut through by calcite veins. **L** Dolomite crystals being severely sheared and tectonized again reflects the recurrence of tectonic events (adapted from Ramkumar et al. 2019)

reference materials DNC-1, W2a, GBW 07,113 (for major and trace elements) and NCS DC70009, OREAS 100a, 101a and 101b (for REEs) were used to ensure accuracy and precision.

The accuracy and precision of the analysis were better than 10%. Geochemical and mineralogical analyses were first grouped according to the field and petrographic facies and further subdivided with variants within each facies. The

statistical analyses examined 33 geochemical constituents for their quantitative measurements using SPSS software, utilizing a standardized dataset with uniform measurement units and PAAS-normalized REE data. Statistical techniques such as correlation and factor analysis were also performed within the same facies and among various facies, grouping according to elemental compositions, the variance of data and dominance of respective elements over total variance (Ramkumar et al. 2006, 2013, 2014). The interpretations derived from these analyses were consequently discussed to assess the parameters influencing the distribution of REE and various elements and reveal the relationships between elemental compositions to identify the potential factors controlling the sources of various elements.

These field, petrographic, geochemical and mineralogical data were used to interpret different phases of dolomitization, to constrain the stages and phases of evolution and their paragenetic sequence. These were then integrated with regional structural trends and stages to evolve an idealistic model on which implications for the geochemical evolution and interaction between host rock and hydrothermal fluids are addressed.

Results

Facies characteristics

The study area LaFarge quarry is located within the Kinta Valley and < 2 km from the eastern flank of the Kledang Range. The Kinta Valley roughly exhibits a "V" shaped morphology. Ramkumar et al. (2019) documented the structural characteristics of the quarry and from the study of the petrographic characteristics of Kinta-Valley carbonates, classified them into seven facies using textural and morphological classification in which six are dolomitic facies and the other is HCM facies and the same are considered for the present study. Textural descriptions adopted terminologies proposed by Friedman (1965), Gregg and Sibley (1984), Sibley and Gregg (1987), and Mazzullo (1992), while that of size description adopted Folk's (1962) size scale (< 30 µm – fine-crystalline, 30–150 µm – medium-crystalline and > 150 µm – coarse-crystalline dolomite). Salient characters of each of these facies types are presented herein.

Host calcareous mudstone (HCM—P1; Fig. 2A and B)

The host rocks are light to dark grey colored thin to thick-bedded, massive (structureless) calcareous mudstones (limestone) (Fig. 1M). The HCMs are non-porous and non-fossiliferous in nature. They are highly fractured. The fractures show multiple orientations (i.e., bedding parallel, tangent and perpendicular). Late-stage calcite and dolomite veins crosscut this facies at different orientations (Fig. 1G). The beds show regional variations in compaction (Fig. 1M). Stylolites are common and can be classified into low-amplitude stylolite and tectonic stylolite (Fig. 2A and B).

Early replacement dolomite (P2; Fig. 2C and D)

This facies is yellowish orange colored dolomite, occurs along the closed fractures which resemble an inverted "V" shape and is formed adjacent to the HCM facies (Fig. 1M and R). Based on the color, texture and mineralogy, these dolomites are considered as the first stage of replacement dolomites. These dolomites consist of polymodal mosaics, medium to coarse transitional planar-e (euhedral) and planar –s (subhedral) to non-planar-a (anhedral) dolomite crystals (Fig. 2C). The planar euhedral [idiotopic mosaic of Friedman (1965); idiotopic-E texture of Gregg and Sibley (1984); and planar-e texture of Mazzullo (1992)] to subhedral dolomite crystals [(hypidiotopic texture of Friedman (1965); idiotopic-S of Gregg and Sibley (1984) and planar-s texture of Sibley and Gregg (1987) and Mazzullo (1992)] are noticed. These are varying in size between 100 and 1000 µm. The non-planar anhedral dolomite crystals [xenotopic texture of Friedman (1965); xenotopic-A texture of Gregg and Sibley (1984); nonplanar texture of Sibley and Gregg (1987) and nonplanar-A texture of Mazzullo (1992)] are 100–2000 µm sized. Most of the dolomites of this facies exhibit straight compromised crystalline boundaries and crystal-face junctions. These dolomites are crosscut by stylolites and calcite veins of different compositions (Fig. 2C). This dolomite facies comprises 65% of the total dolomite by volume in the outcrop. These are considered as replacement dolomites, formed during the first phase of dolomitization based on their thickness, occurrence and contact relationships.

Sucrosic dolomite (P3; Fig. 2F and G)

These are massive in nature and varied in color, (reddish gray and white colored) with sugary texture and formed at the core of the fracture. These are surrounded by the replacement dolomites and exhibit sharp contact with the replacement dolomites. Multi-directional criss-cross fractures (mm thick) and kinks are common in this facies (Fig. 1T). Microscopically, these are polymodal mosaics, coarse to very coarse (200–2000 µm) planar subhedral crystals to non-planar anhedral crystals and medium to coarse (100–400 µm) planar euhedral dolomite crystals (Fig. 2G). Most of the dolomite crystals are tightly interlocked with irregular intercrystalline boundaries with rarely preserved crystal-face junctions and are commonly crosscut by calcite

veins (Fig. 2F). P3 dolomites account for 10% of the total dolomite volume in the outcrop.

Metamorphosed dolomite (P4)

These are formed within the early replacement dolomite facies. Metamorphosed dolomite appears to be a relatively small, massive, pinkish orange geobody, mimics/occupies the morphology of early replacement dolomite facies (P2) and shows sharp contact with early replacement dolomite (Fig. 1U). Minor fractures are common and these fractures are filled with calcite veins.

Late replacement dolomite (P5; Fig. 2H and I)

These are white colored and are located between the early replacement dolomite (P2) and the sucrosic dolomite (P3). They show sharp contacts with the early replacement dolomites (P2) (Fig. 1V). They occur in the dense fractures, which crosscut all other facies. The crosscutting relationship of this dolomitic facies (P5) postdates the early replacement dolomites (P2) filled fractures. The dolomites of this facies are unimodal, coarse to very coarse (1000–2000 µm) planar euhedral to subhedral and non-planar anhedral dolomite crystals (Fig. 2H). This dolomite facies shows closely packed dolomite crystals with irregular intercrystalline boundaries, rarely preserved crystal-face junctions and some with undulatory extinction. In addition, saddle dolomite crystals are common. They range in size from 1000 to 2000 µm non-planar crystals, with a scimitar, or half-moon-like terminations pointing to pore spaces (Fig. 2I). The P5 dolomites comprise 25% of total dolomite by volume of the outcrop.

Late stage calcite (P6; Fig. 2J–L): This calcite facies consists of perfect rhombohedral, transparent calcite crystals which represent the last stage of the diagenetic history of the metamorphosed limestone. They occur within the apex of the fractures as relatively small, massive, dusky white to transparent isolated chunks (Fig. 1W).

Mineralogy

The HCM consists of Mg-Ca carbonate, Mg-calcite, calcium carbonate and calcite. The majority of the HCM samples are high Mg-Ca carbonates (80–100%). The dolomitized phases are enriched in dolomite and by Mg-Ca carbonates. The P2 and P5 samples are exclusively dolomites. The studied carbonates were divided based on XRD quantitative results, which further provide information on the degree of dolomitization. Following the mineralogical classification of Carr et al. (1994), the carbonates are grouped according to their dolomite contents. Accordingly, the studied samples consist of 85% of dolomites and 15% of calcitic dolomites. The carbonates varied from calcitic dolomite in P1 facies to dolomite in P2–P5 carbonate facies.

Geochemistry

A summary of the geochemical analytical results of the studied samples is presented in Table 1 and the complete dataset is presented in Table S1 (Supplementary table S1a–d).

Major oxides

The HCM and calcite (P1 and P6) have relatively higher CaO content (53 Wt% in P1 and 56 Wt% in P6) than the dolomite group of rocks (P2–P5; 38 Wt%, 32 Wt%, 48 Wt% and 32 Wt%). The MgO content is higher in the dolomite group of rocks (16 Wt%, 19 Wt% 6 Wt% and 20 Wt% in P2–P5 facies, respectively) than the HCM and calcite (1 Wt% and 0.23 Wt% in P1and P6 facies, respectively). In general, SiO_2 and Al_2O_3 are < 2 Wt% and 1 Wt%, respectively, in all the studied carbonates. The Na_2O, K_2O, TiO_2 and P_2O_5 are < 0.1 Wt%. Overall, SiO_2, Al_2O_3, TiO_2 and P_2O_5 are higher in the P2 group of samples, while Fe_2O_3, MnO, MgO and Na_2O are higher in the P5 group of samples. P6 ($n = 1$) records the lowest concentration for all the elements and shows the highest contents of CaO. The Fe_2O_3, MnO and MgO contents show a relatively similar decreasing trend as high in P5 and low in P6 samples and are enriched in the dolomite group of samples rather than HCM. PAAS normalized plot shows that the CaO content is depleted while MgO (2–tenfold), and MnO (up to 30-fold) contents are enriched in dolomite samples (P2–P5) than the HCM and calcite (P1 and P6; Fig. 3A).

Trace elements

The trace elements Co, Cr, Ni, Rb, Cs, Zn, Ga, As, Nb, Sn, Ta and W are below the detection limits in most of the samples whilst Be, Ge, Ag, In, Ti, Pb and Bi are below detection limits in all the samples, and hence these elements are not used for the interpretations. Among the trace elements determined, Sr is significantly higher. Yet, a disparity exists such that, Sr is in the range of 159–668 ppm in HCM and it is recorded in the ranges of 32–203; 31–61; 93 and 34–48 ppm in P2–P5 dolomite facies respectively. Next to Sr, the most abundant element is Cu, with average values of 34 ppm in the HCM (P1 facies), 40 ppm in the calcite (P6 facies) and 29, 39, 30 and 30 ppm in the dolomites (P2–P5 facies, respectively). Sc, Ba, Sr, Cr and U are higher in HCM (P1),

Table 1 Descriptive statistics of geochemical parameters for the Kinta Valley carbonate facies types

Para-meters	Host calcareous mudstone (HCM – P1) ($n=9$)				Early replacement dolomite (P2) ($n=11$)				Sucrosic dolomite (P3) ($n=7$)				Metamorp-hosed dolomite (P4) ($n=1$)	Late replacement dolomite (P5) ($n=4$)				Late stage calcite (P6) ($n=1$)	Detection limit
	Min	Max	Mean	SD	Min	Max	Mean	SD	Min	Max	Mean	SD		Min	Max	Mean	SD		
SiO_2	0.24	3.15	1.01	0.93	0.39	2.57	1.18	0.80	0.1	1.64	1.07	0.67	0.13	0.30	0.78	0.64	0.23	0.04	0.01
Al_2O_3	0.14	0.95	0.40	0.29	0.23	1.19	0.61	0.35	0.1	0.87	0.59	0.33	0.11	0.20	0.47	0.39	0.13	0.07	0.01
Fe_2O_3(T)	0.14	0.43	0.26	0.09	0.2	0.6	0.44	0.13	0.22	0.51	0.41	0.12	0.12	0.35	0.75	0.46	0.19	0.05	0.01
MnO	0.03	0.06	0.04	0.01	0.18	0.36	0.26	0.06	0.26	0.34	0.30	0.02	0.13	0.30	0.34	0.32	0.02	0.005	0.001
MgO	0.73	1.96	1.28	0.47	8.4	20.4	15.82	4.44	17.48	21.04	19.24	1.18	6.34	19.61	20.32	19.86	0.32	0.23	0.01
CaO	51.38	55.27	53.36	1.17	30.43	43.46	35.73	4.95	31.18	33.42	32.18	0.78	48.22	30.77	31.81	31.26	0.51	55.6	0.01
Na_2O	0.01	0.01	0.01	0.00	0.01	0.04	0.02	0.01	0.02	0.04	0.03	0.01	0.02	0.03	0.04	0.04	0.01	–	0.01
K_2O	0.01	0.01	0.01	–	0.01	0.02	0.01	0.01	0.01	0.01	0.01	0.00	0.01	0.01	0.02	0.01	0.01	0.01	0.01
TiO_2	0.004	0.04	0.02	0.01	0.02	0.09	0.03	0.02	0.005	0.04	0.02	0.01	0.01	0.02	0.024	0.02	0.00	0.002	0.001
P_2O_5	0.02	0.04	0.03	0.01	0.02	0.13	0.04	0.03	0.02	0.04	0.03	0.01	0.03	0.02	0.04	0.03	0.01	0.02	0.01
LOI	41.87	43.81	43.02	0.62	42.81	46.51	45.02	1.37	44.92	47.04	45.60	0.93	44.13	46.08	46.63	46.23	0.27	43.31	–
Sc	1	2	1.33	0.58	1	2	1.25	0.46	1	1	1.00	0.00	–	1.00	1	1.00	0.00	–	1
V	5	9	7.20	1.64	5	12	7.27	1.95	5	9	7.57	1.51	–	5.00	7	6.33	1.15	–	5
Ba	8	16	12.33	2.40	4	7	5.36	1.29	4	5	4.43	0.53	6.00	3.00	5	4.25	0.96	4	3
Sr	159	668	418.44	145.35	32	203	80.73	52.94	31	61	45.71	10.11	93.00	34.00	48	39.75	6.95	17	2
Y	5	19	11.00	3.81	6	23	14.82	4.62	11	15	12.86	1.57	9.00	6.00	17	10.50	5.07	6	2
Zr	5	17	8.67	4.24	7	94	19.91	25.07	4	17	11.57	5.00	5.00	9.00	13	10.75	2.06	–	4
Cr	20	20	20.00	–	20	20	20.00	0.00	20	20	20.00	0.00	–	20.00	20	20.00		–	20
Co	2	2	2.00	–	–	–	–	–	–	–	–	–	–	–	–	–	–	–	1
Ni	20	20	20.00	–	30	30	30.00	–	–	–	–	–	–	–	–	–	–	–	20
Cu	30	50	34.44	7.26	20	50	29.09	9.44	30	50	38.57	6.90	30.00	10.00	50	30.00	16.33	–	10
Zn	–	–	–	–	60	60	60.00	–	–	–	–	–	–	–	–	–	–	–	30
Ga	1	1	1.00	–	1	2	1.40	0.55	1	1	1.00	–	–	–	–	–	–	–	1
As	6	6	6.00	–	–	–	–	–	–	–	–	–	–	–	–	–	–	–	5
Sn	–	–	–	–	1	1	1.00	–	–	–	–	–	–	–	–	–	–	–	1
Hf	0.2	0.4	0.30	0.14	0.3	1.9	0.70	0.67	0.3	0.4	0.32	0.04	–	0.20	0.3	0.25	0.07	–	0.2
Ta	–	–	–	–	0.1	0.1	0.10	–	–	–	–	–	–	0.00	0	–	–	–	0.1
W	2	2	2.00	–	1	1	1.00	–	–	–	–	–	–	1.00	1	1.00	–	–	1
Th	0.2	1.3	0.66	0.37	0.7	3	1.26	0.72	0.2	1	0.70	0.32	0.40	0.50	0.8	0.70	0.14	0.1	0.1
U	0.1	0.9	0.49	0.26	0.2	1.1	0.47	0.29	0.1	0.6	0.40	0.19	0.20	0.10	0.2	0.18	0.05	0.1	0.1
La	5.1	16	8.98	3.36	3.8	17.6	9.06	3.87	3.9	12.6	8.43	3.50	7.20	5.10	6.6	5.83	0.69	2.7	0.1
Ce	5.1	16.9	8.77	3.83	4.1	25.9	10.85	5.98	5.6	8	6.86	1.08	6.30	4.30	11.3	6.68	3.20	0.7	0.1
Pr	0.95	3.34	1.70	0.73	0.84	3.74	2.19	0.78	1.12	2.74	1.93	0.68	1.42	0.94	2.23	1.41	0.60	0.52	0.05

Table 1 (continued)

Para-meters	Host calcareous mudstone (HCM – P1) ($n=9$)				Early replacement dolomite (P2) ($n=11$)				Sucrosic dolomite (P3) ($n=7$)				Metamorp-hosed dolomite (P4) ($n=1$)	Late replacement dolomite (P5) ($n=4$)				Late stage calcite (P6) ($n=1$)	Detection limit
	Min	Max	Mean	SD	Min	Max	Mean	SD	Min	Max	Mean	SD		Min	Max	Mean	SD		
Nd	3.5	13.4	6.83	2.99	3.6	15.6	9.25	3.17	4.8	10.8	8.07	2.57	6.00	3.80	9.9	6.03	2.81	2.1	0.1
Sm	0.7	2.9	1.41	0.69	0.7	3.2	1.99	0.65	1.1	2	1.60	0.38	1.20	0.80	2.4	1.35	0.75	0.4	0.1
Eu	0.23	0.51	0.34	0.11	0.17	0.64	0.39	0.13	0.21	0.46	0.34	0.10	0.26	0.17	0.34	0.24	0.08	0.09	0.05
Gd	0.7	3	1.52	0.70	0.7	3.1	2.04	0.65	1.2	2	1.63	0.30	1.30	0.80	2.5	1.40	0.78	0.5	0.1
Tb	0.1	0.5	0.25	0.13	0.1	0.5	0.31	0.10	0.2	0.3	0.24	0.05	0.20	0.10	0.4	0.20	0.14	–	0.1
Dy	0.6	2.6	1.38	0.63	0.7	2.7	1.83	0.58	1.2	1.7	1.44	0.22	1.20	0.70	2.2	1.25	0.69	0.4	0.1
Ho	0.1	0.5	0.28	0.12	0.1	0.5	0.35	0.13	0.2	0.4	0.29	0.07	0.20	0.10	0.4	0.25	0.13	–	0.1
Er	0.3	1.3	0.73	0.30	0.4	1.5	1.01	0.32	0.7	0.9	0.80	0.10	0.70	0.40	1.2	0.70	0.36	0.2	0.1
Tm	0.06	0.18	0.11	0.04	0.06	0.2	0.14	0.05	0.1	0.13	0.11	0.01	0.09	0.05	0.16	0.10	0.05	–	0.05
Yb	0.2	1	0.61	0.24	0.4	1.2	0.84	0.28	0.6	0.7	0.66	0.05	0.60	0.30	0.9	0.58	0.28	0.2	0.1
Lu	0.05	0.15	0.10	0.03	0.05	0.18	0.12	0.04	0.09	0.11	0.10	0.01	0.09	0.05	0.13	0.08	0.04	–	0.04
∑REE	29.65	73.26	45.29	13.87	19.72	72.14	45.72	14.52	25.24	47.07	36.93	8.64	32.76	22.47	43.66	30.33	9.81	11.81	NA
Ce/Ce*	0.40	0.61	0.51	0.07	0.34	1.49	0.59	0.30	0.31	0.77	0.44	0.17	0.45	0.44	0.67	0.52	0.09	0.14	
Eu/Eu*	0.99	2.69	1.28	0.63	0.69	1.14	0.92	0.14	0.86	1.12	0.99	0.09	0.98	0.65	1.00	0.88	0.14	0.95	
Mn*	0.93	1.43	1.17	0.16	1.44	1.12	1.71	0.22	1.66	2.12	1.81	0.16	1.97	1.58	1.90	1.80	0.12	0.93	

(– = BDL/Below Detection Limit; *SD* standard deviation, *NA* not applicable); Major oxides in Wt% and trace and rare earth elements are reported in ppm. $Ce/Ce^* = (Ce_{SN}/(0.5^* La_{SN} + 0.5^* Pr_{SN})$, Elderfield and Greaves (1982); Eu/Eu^*: $Eu_{SN}/[(Sm_{SN})(Gd_{SN})]^{1/2}$, Taylor and McLennan (1985); $Mn^* = \log[(Mn_{sample}/Mn_{shale})/(Fe_{sample}/Fe_{shale})]$, Bellanca et al. (1996)

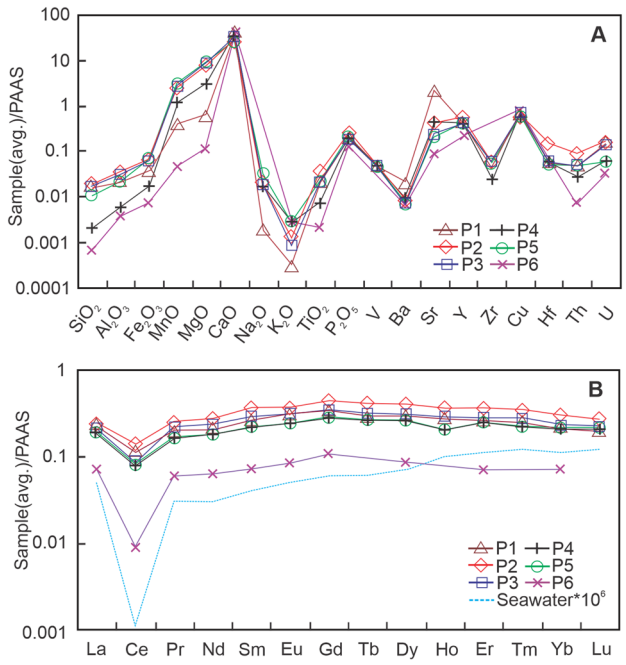

Fig. 3 **A** PAAS normalized multi-element plots of the Kinta Valley Carbonates (P1-host calcareous mudstones (HCMs); P2-P5dolomites; and P6-calcite vein; **B** PASS normalized REE pattern of the Kinta Valley carbonates (Seawater reference curve; retrieved from Zhang et al. 2014; calculated from Alibo and Nozaki 1999 and magnified 10^6 times)

while V, Y, Zr, Hf and Th are higher in P2 group dolomites (Fig. 3A). Except for Cu, other elements are depleted in late calcite facies (P6). Among the trace elements, Sr is depleted in dolomites than limestone with a fluctuation in P2 dolomites. Except for Cu, other elements are recorded below the average shale values.

Rare earth elements (REE)

The shale normalized REE pattern of each facies displays a parallel to sub-parallel (nearly flat) shape and does not show any fractionation (Fig. 3B) despite a relative enrichment of MREE. The ∑REEs display a significant variation between the HCM and the calcite (mean 45 ppm in P1; 12 ppm in P6) and dolomites (46, 37, 33 and 30 ppm in P2–P5 facies, respectively). Overall, the ∑REEs decrease from P2 to P5 facies. The REE characteristics of carbonates of the Kinta Valley, in comparison with that of seawater, feature the following properties: (a) slight LREE depleted/partially enriched pattern (average $(Nd/Yb)_{SN}$ ratio as 0.97 ± 0.26 in P1; 0.93 ± 0.18 for P2; 1.01 ± 0.26 for P3; 0.83 for P4, 0.90 ± 0.17 for P5 and 0.87 for P6; Seawater Nd/Yb_{SN} ratio = 0.205 to 0.497 for 50 m depth); (b) true negative Ce_{SN} (except 1 sample 5C-P2 facies) and positive La_{SN} anomalies (Fig. 4A; Ce/Ce* = 0.51; 0.50; 0.44, 0.45, and 0.14 in P1–P6 facies, respectively; < 0.1 to 0.4 for seawater; Elderfield and Greaves 1982; Piepgras and Jacobsen 1992); (c) Positive Gd_{SN} anomalies (1.24 ± 0.45; 1.10 ± 0.19; 1.13 ± 0.27; 1.06; 1.48 ± 0.53) in P1—P5 facies, respectively; [Seawater ~ 1.05–1.30; Zhang and Nozaki 1998; Nothdurft et al. 2004; Vietnam Shelf, western South China Sea (Gd/Gd* = 1.3–1.4; Nguyen et al. 2013). The Gd anomaly of the South China Sea water is influenced by the western North Pacific seawater and thus shows a relatively negative Gd anomaly (Gd/Gd* = 0.88; Amakawa et al. 2000; Li et al. 2019a, b)] and (d) super chondritic Y/Ho ratios (avg. 42, 44, 46, 45, 44 for P1–P5 facies, respectively; [~ 44 to 74 in seawater; Bau 1996; Nozaki et al. 1997; 40–80 in open marine settings; Bau et al. 1997], which are comparable to the REE pattern of the seawater (Nothdurft et al. 2004 Nagarajan et al. 2011; Tostevin et al. 2016; Subramanyam et al. 2020). However, the ratios of many samples are different from the seawater character; in particular, LREE is enriched (Fig. 4B, C). HCM shows LREE enriched (Field B: $(La/Sm)_{SN} > 1$, $(Gd/Yb)_{SN} > 1$,) and dolomitic facies mainly fall in the field A (Field A: $(La/Sm)_{SN} < 1$,$(Gd/Yb)_{SN} > 1$, MREE enrichment). Nevertheless, the majority of the samples show true negative Ce and positive Eu anomalies (Fig. 4A, B).

Discussion

Geochemical characteristics of HCM (P1) and dolomites (P2–P5)

The relationships and differences between the studied parameters of the HCMs and dolomitized phases were tested through factor analysis. In this study, only the factor scores with an Eigen value > 1 resulting from varimax rotation are considered for interpretation. The factor analysis has returned six principal factors explaining 97% of total variance with communalities of 0.80 and above for all the studied parameters of the HCM (Table S2). Factor 1 is loaded with many detrital elements (except MgO, Ba, Sr, Zr, Cu, Eu, U) and negatively loaded with CaO, LOI and Eu/Eu*. It indicates the prevalent dominant control of detrital influx (probably represented by aluminosilicates as revealed by XRD as well as petrography described previously) over the depositional conditions. The inference of influx of aluminosilicates is affirmed by the positive correlations of Al_2O_3 with other elements and negative correlation of CaO with SiO_2 and Al_2O_3 (e.g. Nothdurft et al. 2004; Zhao and Zheng 2014; Li et al. 2019a, b). The Kinta carbonates are interbedded with clastic materials or argillaceous units as a calcareous subordinate of schists and phyllites (Kadir et al. 2011) and shales (Gebretsadik et al. 2017). These might have been the sources of these aluminosilicates during the deposition

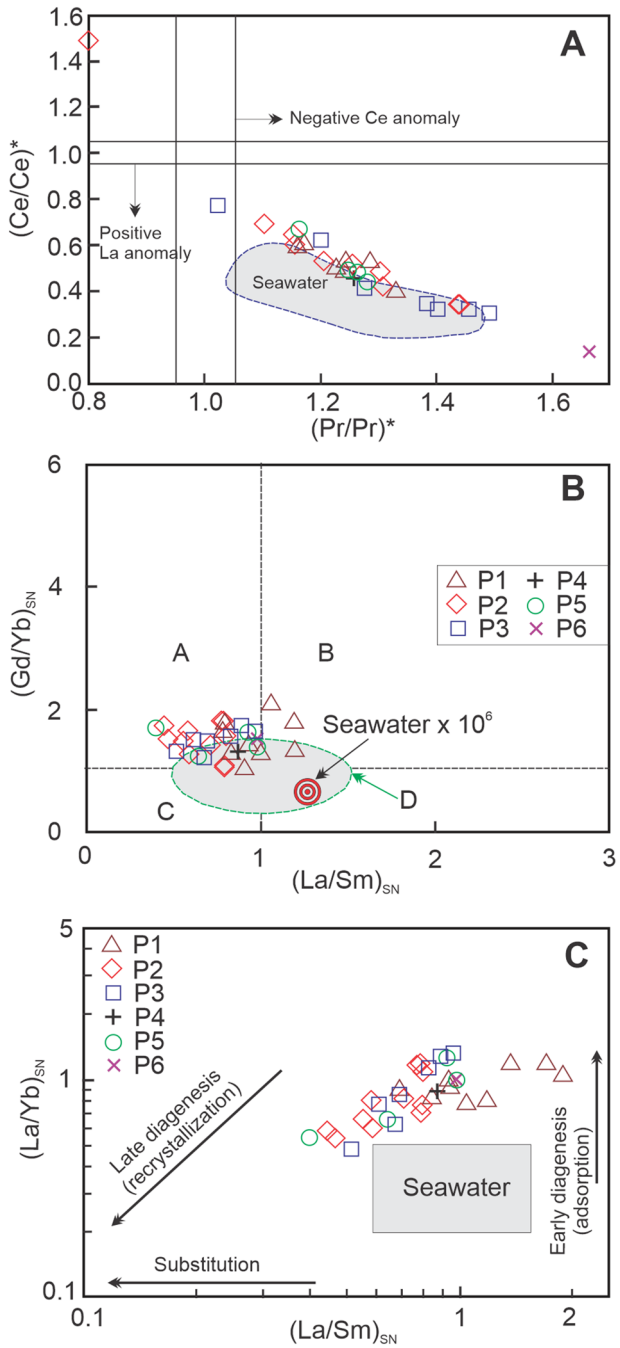

Fig. 4 **A** Binary diagram of Ce/Ce* vs Pr/Pr* (after Bau and Dulski 1996) shows the anomaly fields for Kinta valley Carbonates. The shaded region shows the range of modern seawater. **B** The plot of Gd/Yb against La/Sm for discrimination of REE distribution patterns. Field **A**: $(La/Sm)_{SN} < 1$, $(Gd/Yb)_{SN} > 1$, MREE enrichment; Field **B**: $(La/Sm)_{SN} > 1$, $(Gd/Yb)_{SN} > 1$, LREE enrichment; Field **C**: $(La/Sm)_{SN} < 1$, $(Gd/Yb)_{SN} < 1$, HREE enrichment; Field **D**: $(La/Sm)_{SN} \sim = 1$, $(Gd/Yb)_{SN} \sim = 1$, flat REE pattern and **C**. Effects of diagenesis were analyzed using a diagram proposed by Reynard et al. (1999). Dolomite samples show a decreasing trend of $(La/Yb)_{SN}$ ratios, interpreted as a progressive mechanism of REE recrystallization onto the carbonate lattice during late diagenesis

of the HCMs. This factor alone explains 48.5% of the total variance and unequivocally establishes the preservation of pristine, depositional signatures despite extended diagenetic and other events that followed since deposition.

Factor 2 represents 16.7% of the total variance. It is positively loaded with Sr, Eu and elemental ratios (Y/Ho, Eu/Eu*, Gd/Yb and La/Yb). The positive loadings of Sr and Eu in this factor can be related to detrital feldspars. However, Eu/Eu* anomaly shows a moderate negative correlation with the majority of the elements and positive correlations with CaO and Sr ($r = 0.66$; 0.54, respectively). This may indicate that the Eu anomaly is not masked by terrigenous input and the studied samples retain seawater characters or influence of hydrothermal activities without significant obliteration. Factor 3 explains 9.7% of the total variance. It is positively loaded with MgO, TiO_2 and Zr, indicating control of these elements by aluminosilicates/dolomitization represented by either heavy mineral fraction and/or Mg-phyllosilicates. The mineral zircon appears to control the REE content of the HCM, in particular HREEs (Zr Vs HREE; $r = 0.56$). The presence of these elements has partially influenced the seawater REE pattern; i.e. Y/Ho ratio and La/Sm ratio. Factor 4 represents 7.3% of the total variance and is explained by positive loadings of Fe_2O_3, Th and Ce/Ce*. These indicate that the seawater Ce anomaly has been modified by the Fe-oxides and Th resulting in increased Ce/Ce* values > 0.4 in the studied HCMs (e.g. MacLeod and Irving 1996; Tostevin et al. 2016). However, the Ce anomalies of the limestones have been influenced by the detrital input and Fe-oxides. These explain the enriched Ce anomaly. On the other hand, positive Ce anomaly (Sample Number 4YA; Ce/Ce* = 1.48) is developed by the influence of Fe oxide-rich oxic sediments, for instance, red clay (Piper 1974b; Toyoda et al. 1990; Nagarajan et al. 2011) and cherts (Slack et al. 2007; Planavsky et al. 2010). At this juncture, the presence of minor hematite confirmed in XRD analysis is noteworthy. Factor 5 is explained by positive loadings of Cu and U, which may have been controlled by either sulphide phases or redox conditions. However, other redox-sensitive elements are not loaded in this factor. Thus, this behavior may not represent redox conditions during the deposition of the HCM. Factor 6 is positively loaded with Ba, Sr and negative loading of P_2O_5, which can be related to diagenetic fluids.

The dolomites are distinct from the HCM by enrichment of MgO. During this process of substitution/replacement and/or preferential accumulation of Mg, the elements such as Sr, Ba, Ca and U were also expelled as indicated by their negative correlations with MgO. However, Na_2O and MnO contents of the dolomites show affinity with dolomitization. Though the chemical characteristics of the HCMs are modified during the dolomitization process, relict features are recorded. That is, the geochemical signatures associated with detrital phases, aluminosilicates and heavy minerals

are preserved. However, REEs of dolomites do not show strong relationships with any detrital elements. Although, a weak positive correlation exists between the LREEs with the Si and the Al. A similar association is observed in HCMs, where concentrations of the REEs were mainly influenced by HREEs together with Zr, TiO_2, V, Th and U. In particular, U is associated with the REE contents in the HCM. Variations in the relationships of elements in dolomites can be related to variations in the effect of dolomitization, which are discussed herein.

The factor analysis of the dolomitic phases using principal components with varimax rotation returned five principal factors, explaining a total variance of 89.17% with communalities above 0.75 for most of the parameters except for Cu (communalities = 0.51) and Fe_2O_3 (communalities = 0.61) (Table S3). Factor 1 explains 41.51% of the total variance with the positive loadings of REEs and Y indicative of the preserved seawater characteristics of precursor HCMs and uninfluenced by later-stage diagenetic fluids. Factor 1 is also explained by moderate positive loadings of U, which indicates redox conditions of the seawater. Factor 2 explains 16.85% of the total variance with the positive loadings of Si, Al, Ti, P, V, Zr and Th, suggestive of terrigenous fraction-controlled nature (Ganai et al. 2018; Li et al. 2019a, b). The association of these elements with detrital fractions correlates to the preserved depositional signatures of the precursor HCM in the dolomites. However, few of the trace elements may also have been controlled by the diagenetic fluids as selected elements can be remobilized from carbonate and non-carbonate fractions (Ganai et al. 2018). Factor 3 has negative loadings of Mn, Mg and Na and positive loadings of Ca, Ba and Sr. This characteristic indicates that the elements Mn, Mg and Na have substituted Ca, Ba and Sr during dolomitization, perhaps under high temperatures (e.g. Stanley 2008). Higher Na contents in dolomites show coherent nature with Mg and Mn in the studied samples, which is oblivious to the common occurrences of depletion of Na in carbonates during diagenesis and implies similar diagenetic fluids enriched with Na. Factor 4 represented by positive loading of Eu anomaly, Cu, Th, Al and Si indicates that the positive Eu anomaly formed by the effect of hydrothermal input in HCM might have been modified by minor suspended solids introduced from diagenetic fluids. Factor 5 explains 5.94% of the total variance. It is represented by positive loadings of Ce anomaly and Ce, and negative loading of Fe_2O_3. It indicates the unrelated nature of the Ce-anomaly with the Fe-Oxides and dolomitization processes.

Geochemical signatures of the HCM (P1) and depositional conditions

The presence or absence of Ce anomalies in ancient marine authigenic sediments (Elderfield and Greaves 1982; Liu et al. 1988; Nagarajan et al. 2011; Li et al. 2019a, b) help interpret palaeo-redox variations in the ancient oceans. Distinct negative Ce anomalies are shown in carbonate minerals precipitated in equilibrium with seawater and this may also be observed in the bulk REE pattern (Piper 1974a; Palmer 1985). Their occurrences indicate the incorporation of REEs into the mineral phases directly from seawater or pore water under oxic conditions (Elderfield and Greaves 1982; Liu et al. 1988; Nagarajan et al. 2011; Tostevin 2021).

A bivariate plot has shown the occurrences of La anomaly and Ce anomaly (Fig. 4A; Bau and Dulski 1996). The samples of HCM in this discrimination plot (Pr/Pr* vs. Ce/Ce*) show original negative Ce anomalies and positive La anomalies and are almost compatible with the modern seawater (Fig. 4A) with a slight deviation. Similarly, a strong negative correlation exists between the CaO and the ∑REEs affirming seawater origin and preservation of depositional signature without much obliteration.

The HCMs exhibit a negative Ce anomaly resembling that of the seawater, but relatively higher Ce/Ce* values than that of typical seawater values (average Ce/Ce* ratios: P1: 0.51, P2: 0.58, P3: 0.44; P5: 0.52) with small variations in their range (Table 1). Together, they imply that the bottom water oxygen level was stable and did not fluctuate too much. However, when compared with the Ce/Ce* values of the seawater (< 0.1 to 0.4; Elderfield and Greaves 1982), the samples under study show relatively higher Ce/Ce* values and suggest prevalent mixing of detrital clay with marine sediments. The superchondritic Y/Ho ratios for the analyzed carbonates (32.2–59.4) fall within the range of seawater (Y/Ho = 44 to 74; Bau 1996; 60–90; Lawrence et al. 2006) except few samples, which show lower values. The values are also significantly different from the open-ocean seawater and nearshore environments (Y/Ho ratio 108 and 94, respectively; Nozaki et al. 1997). The lower values are comparable to the Y/Ho ratio of the terrigenous materials and volcanic ash, which show a constant ratio of ~ 28. The occurrences of excellent correlations between the Y and Ho concentrations of the studied samples ($r = 0.93$ for HCMs; $r = 0.90$ for dolomites) imply that the fluids in which these carbonates were stabilized have similar Y/Ho ratios (e.g. Zhao and Jones 2013). The Y/Ho values of many HCM samples represent the seawater range except few samples. The fluctuations of Y/Ho ratios of the HCM reflect a possible change in the ratios by terrigenous input as suggested by the detrital elements, which have changed the Y/Ho ratio of seawater. However, a narrow range of Y/Ho points toward a relatively stable tectonic environment.

Carbonates with enriched ∑REEs could be related to the contamination by oxides, sulphides, phosphates or silicates, derived from either terrestrial particulate matter (shale) and/or hydrothermal input (Frimmel 2009). The mean ∑REE of HCM in the studied samples (7.8–62.3 ppm) is higher

than other Paleozoic marine carbonates (e.g. Wang et al. 2009), with more than 90% of samples showing ∑REE content > 20 ppm, which further supports detrital input. A minor REE contribution from shale as little as 1–2% could significantly affect the La and Ce anomalies, and hence, the REE pattern recorded in the marine carbonates is considered altered resulting in flat, uniform shale-normalized patterns due to the relatively high content of REEs in shale (Nothdurft et al. 2004; Ganai et al. 2018) than that of in seawater. Subsequently, altered seawater-like REE distribution with the majority of the samples exhibiting LREE enrichment and flat REE pattern recorded in HCM reflects modification due to shale contamination.

The Si, Al, Ti and Mn show strong to moderate positive correlations with the REEs. The correlations among detrital minerals signify the presence of terrigenous input during deposition. These could be interpreted as the result of an influx of significant additional sources for LREE and thus modified seawater REE pattern (e.g. Nothdurft et al. 2004; Frimmel 2009; Delpomdor et al. 2013). Insoluble elements in natural waters (i.e. Ti, Al, Zr, Nb, Hf, Ta and Th) have shorter residence times than in ocean and low seawater/crust distribution coefficients (Taylor and McLennan 1985). These elements are rich in shales and abundant in various detrital minerals, for instance, zircon and clay minerals (Frimmel 2009; Ganai et al. 2018; Li et al. 2019a, b) and thus useful to detect the degree of contamination by terrestrial particulate matter and shale into the carbonate system (Frimmel 2009; Ganai et al. 2018; Li et al. 2019a, b). The SiO_2, Al_2O_3, TiO_2, Th, Fe_2O_3 and MnO show moderate correlation with most of the REEs and ∑REEs ($r = 0.93$, 0.85, 0.76, 0.60, 0.59 and 0.62, respectively). These, together with variation in the ∑REEs indicate the input of non-carbonate aluminosilicates during the deposition of the HCMs (e.g. Srivastava and Singh 2019). In addition, P_2O_5 shows a weak positive correlation with ∑REEs and implies control of the REE content in the limestones by the presence of apatites (phosphates).

Diagenesis

Significant depletion of Sr and enrichment of Mn in the diagenetic carbonate phase are expected during the diagenetic transformation of marine carbonates (Veizer 1983a, b; Kaufman and Knoll 1995). Thus, the correlation between the Sr and Mn can be useful to understand the diagenetic alteration in the carbonates (Brand and Veizer 1980; Ganai et al. 2018). The ratio of Mn/Sr can be used to assess the effect of diagenesis or the degree of carbonate preservation against diagenesis (Veizer 1983a,b; Kaufman and Knoll 1995; Delpomdor et al. 2013). The plot of Mn against Sr shows a strong negative correlation for dolomites while a weaker correlation in the HCMs (Fig. 5A). Diagenetically affected dolomites show significant enrichment in Mn (> 1000 ppm vs few 100 s ppm in the HCM (P1) and 39 ppm in P6 calcites) and depletion of Sr (< 100 ppm in dolomites from 668 to 159 ppm in HCMs). These observations suggest that the dolomites are highly altered by diagenesis than the limestones. According to Bartley et al. (2001) the characteristics of non-diagenetic carbonate sediments are: Mn/Sr ≤ 3 and Rb/Sr ≤ 0.01 (dolomites) and Mn/Sr ≤ 1 and Rb/ Sr ≤ 0.01 (limestones). In the present study, both HCMs and selected dolomites are considered unaltered as they have the similar elemental ratios that of non–diagenetic carbonates as reported by Bartley et al. (2001). Accordingly, the majority of the HCMs (Mn/Sr: 0.4–2.5; P1) are unaltered except for two samples that show ratios > 1. On the other hand, P2 dolomites (Mn/Sr: 6.8–74.5) are less altered compared to the P3 (Mn/Sr: 33.5–85.4) and P5 dolomites (Mn/Sr: 49–77).

Higher Sr/Ca ratios in open diagenetic systems reflect intensive rock-water interaction while Sr/Ca ratios in semi-closed diagenetic systems tend to stay consistent due to low rock–water interaction and limited changes in various diagenetic stages with respect to pristine carbonates (Brand and Veizer 1980; Veizer et al. 1990). The P3 and P5 dolomites show consistent Sr/Ca ratios while P2 dolomites show two clusters, which indicate variable diagenetic stages (early and late) with respect to the HCMs (P1) (Fig. 5B). The occurrence of thermogenic calcite during the last phase of diagenesis points toward a closed system and exhaustion of magnesium supply. The Sr/Ca against Mn plot reveals an open system in the dolomitization phases (Fig. 5B). As the water/rock ratio could represent the openness of the diagenetic system (Brand and Veizer 1980) and the higher water/rock ratios during late diagenesis imply open diagenetic systems. The open diagenetic system implies less extensive water–rock interaction where diagenetic fluid evolves due to constant dissolution–precipitation processes and enrichment or depletion of elemental compositions in diagenetic fluid dependent on distribution coefficient, but to a lesser extent than that in closed systems (e.g. Mehmandosti and Adabi 2013). This is consistent with the geochemical trends as described in previous sections and preceding paragraphs. The P2 dolomites show two clusters where the second cluster overlaps with P3 and P5 dolomites. This implies that the dolomites experienced less extensive water and rock reactions in a more open system. The semi-closed/open dolomitization system could be explained to have formed as a result of faults, fractures and stylolites created during tectonic events and subsequent episodic dolomitization(s) that allowed intermittent connectivity and fluid flow (Lonne and Al-Aasm 2000; Ramkumar et al. 2019). Large variations of water composition within facies could point towards the implication of a low water–rock ratio and a closed system of disequilibrium during dolomitization in which diagenetic water constantly changed its composition due to extensive water–rock interaction. These might result in concentration

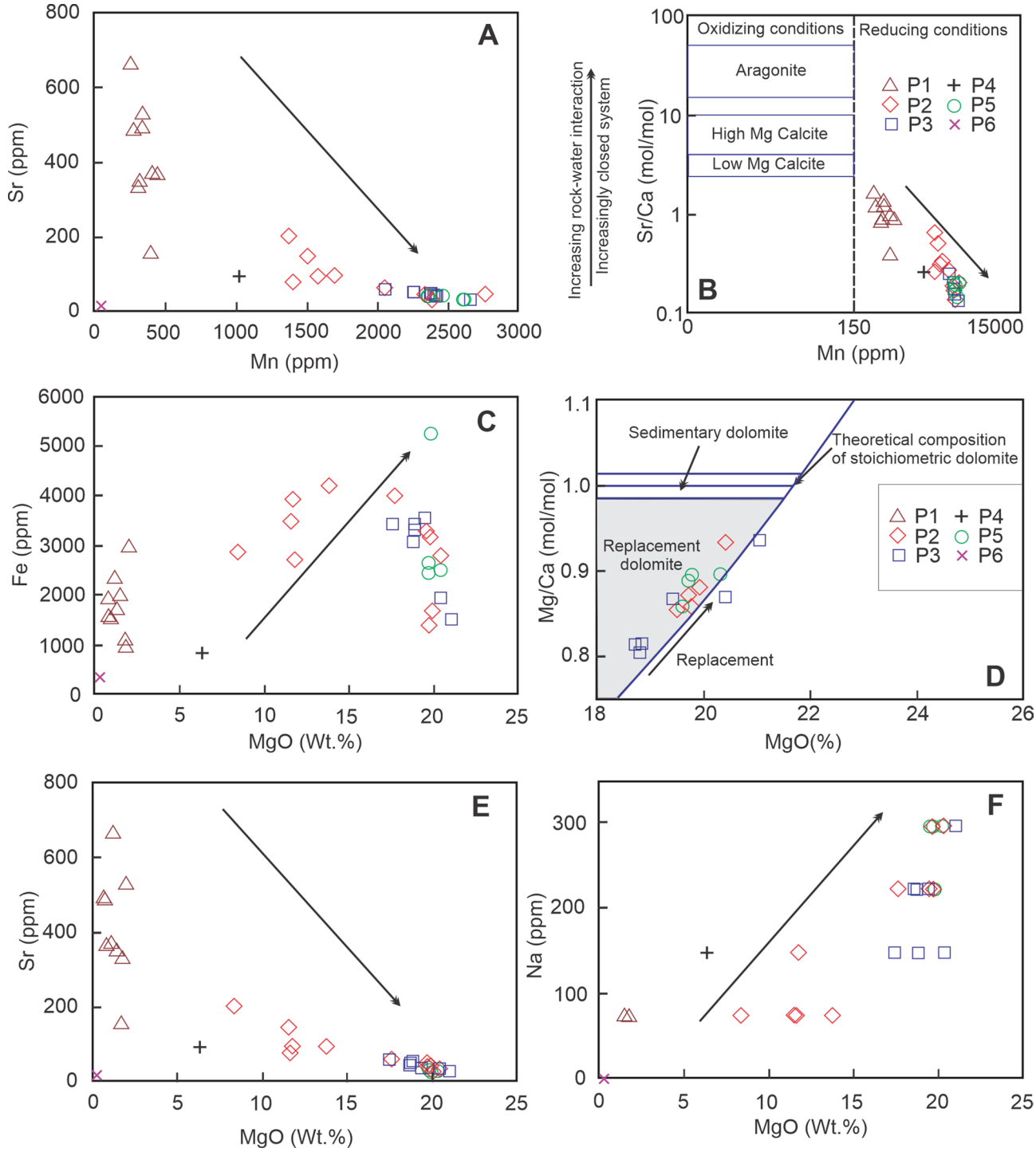

Fig. 5 **A** Mn against Sr plot shows the diagenetic trend for the Kinta carbonates. **B** Sr/Ca ratio against Mn is plotted to determine the diagenesis pattern in a closed and open system (Brand and Veizer 1980). Sr/Ca ratio is increased with an increasing reaction between water and rock while an increase of Mn content in diagenetic calcite implies of open system and the effect of reduction waters (Cicero and Lohmann 2001). **C** The plot of Fe against MgO shows the variation of Fe content; shows an increasing trend in some of the samples (P2) while others show a declining trend with increasing recrystallization. **D** The plot of Mg/Ca against MgO for discrimination of dolomite type (Warren 2000; Chen et al. 2010). **E** The plot of Sr against MgO shows the variation of Sr content with dolomite stoichiometry. **F** MgO against Fe plot shows increasing Na concentration in the dolomites with increasing MgO content. (The arrow on the diagram indicates the diagenetic trend)

gradients of trace elements (a wide range of values) within the studied samples (Veizer 1983b). Hence, the relatively wider range of values in only P2 dolomites pointing to a low water–rock ratio is consistent with the plot showing a relatively closed diagenetic system with higher rock–water interaction. The inverse relationship between Sr/Ca with Mn (Fig. 5B) indicates depleting Sr with increasing stoichiometry. Thus, increasing crystal size and increasing non-planar crystal boundaries suggest diagenetic alteration (recrystallization) of early non-stoichiometric dolomite (e.g., Kupecz et al. 1993; Kupecz and Land 1994), under burial conditions (e.g., Kirmaci and Akdag 2005). Higher Mn values in various diagenetic phases also imply a more open diagenetic system, yet under reducing conditions (Brand and Veizer 1980; Cicero and Lohmann 2001) as reducing conditions favor incorporation of Mn in the carbonate lattice (Shanmugam and Benedict 1983). The gradual enrichment of Mn contents (Fe not exclusively) in the different phases of dolomites (Fig. 5A–C) may be due to a slow change of the diagenetic environments as progressive burial resulting in more reducing conditions and increasing diagenesis (e.g., Veizer 1983a,b; Azmy et al. 2011).

Dolomitization

The predominantly calcitic HCM facies (P1) (Fig. 1M, 2A and B) contains low MgO (0.8–2%; mean = 1.28%) and higher CaO contents (51–55%; mean = 53%). It signifies the absence of broad-scale dolomitization owing to the occurrence of a stable calcite phase. The wide range of MgO content in P2 dolomitic limestone (8.4–20.4%) reflects a varied degree of dolomitization in this dolomite group. The range overlaps a few of the P2 dolomitic limestone (Figs. 1R, 2C) P3 dolomitic limestone (Figs. 1T, 2G) and P5 dolomitic limestone (Figs. 1V, 2H). This observation, together with the narrow range of MgO contents (17.48–21.04% (P3); 19.61–20.32% (P5)) implies a similar degree of dolomitization at a later stage. This phenomenon is common as non-stoichiometric dolomites are susceptible to further diagenetic modification due to their metastable state (i.e., Sibley et al. 1994; Chai et al. 1995; Zhao and Jones 2012). The CaO contents of the dolomites allow the grouping of dolomites into two populations. This grouping signifies that the dolomites underwent varied dolomitization stages, i.e., early stage of dolomitization (weaker intensity) and late stage of dolomitization (higher intensity). The P2 dolomites (early replacement dolomite) exhibit mixed groups of lower calcian dolomites and higher calcian dolomites (30.43–43.46%), while P3 and P5 dolomites (Sucrosic and late replacement dolomite) are classified as low calcian dolomites with CaO contents of 31.18–33.42 and 30.77–31.81%, respectively. This is in line with the dolomite synthesis experiments of Kaczmarek and Sibley (2011) that espoused the calcian dolomitic nature of the early stage of dolomitization under high-temperature conditions. The control exerted by Mg/Ca ratio of the diagenetic fluids for Ca % of the dolomites (e.g., Zhao and Jones 2012) is also demonstrated by the calcian nature of the studied samples. The Kinta carbonates are interpreted to be selectively dolomitized and altered by hydrothermal dolomitization (Ramkumar et al. 2019; Mohammad Zahir et al. 2020; Xin Hui et al. 2021). These studies add support to the inferences on calcian dolomites which are the major control of dolomitization.

The dolomites are categorized as secondary dolomites and further analyzed to differentiate replacement dolomites through a scatter plot of Mg/Ca against MgO (Fig. 5D; Warren 2000; Chen et al. 2010). The dolomite samples fall in the replacement dolomite field along the replacement line with a positive correlation, which affirms the replacement origin. During dolomitization of limestones, the Ca^{2+} will be substituted by Mg^{2+} and the composition of limestone becomes progressively stoichiometric and thus those samples close to stoichiometry fall along the replacement line (e.g. Chen et al. 2010; Zhang et al. 2014). The Sr versus MgO plot shows a decreasing trend for Sr with increasing MgO (Fig. 5E), due to the non-stoichiometric nature of the dolomites (Rahimi et al. 2016). The Sr content in dolomites decreases with increasing stoichiometry (Vahrenkamp and Swart 1990). For instance, more stoichiometric P3 dolomites have 21% of MgO and 31 ppm of Sr, whereas less stoichiometric P2 dolomites contain 8.4 wt% of MgO and 203 ppm of Sr, respectively. The gradual depletion of Sr contents in the studied samples could be explained by the progression of dolomites towards stoichiometry via dissolution and reprecipitation, with a lower effective partition coefficient during progressive stabilization (Land 1980; Veizer 1983a, b; Qing and Mountjoy 1989; Kupecz and Land 1994). Huang et al. (2006) interpreted the low concentration of Sr in dolomites due to precipitation of dolomites from low Sr fluids, or it was difficult for Sr to be incorporated into the dolomite lattice during dolomitization. On the other hand, the primary mineral being replaced with dolomite and its Sr content plays the main role (Veizer 1978). Higher contents of Sr could be observed in replacement dolomites originating from aragonites than those originating from the calcite (Rahimi et al. 2016). However, aragonite is absent in the Kinta carbonates, and there are no indications of their prevalence even at depositional times and thus the primary mineralogy before the replacement of dolomites affecting the Sr values was not taken into account.

In general, Sr and Na are depleted during post-depositional diagenesis of carbonates, especially in late diagenetic dolomites, while Mn and Fe are enriched (Brand and Veizer 1980; Veizer1983a, b). The rationale for this phenomenon is the occurrences of lesser concentrations of Fe and Mn in seawater than in diagenetic fluids (Tucker and Wright 1990)

and higher concentrations of Fe and Mn in diagenetic fluids in reducing conditions (Warren 2000; Ramkumar 2007, 2008). In the present study, only Mn is enriched with Mg but Fe is not enriched. Fe does not show any correlation either with Mn or MgO (Fig. 5C), which indicates Fe content in the studied dolomites was not controlled by the dolomitization. The rise of Mn concentration in dolomite than the limestone can be related to the substitution of Mn for Mg (Rahimi et al. 2016). Mn is preferentially incorporated into the carbonate lattices during diagenesis because the distribution coefficients in carbonates are greater than 1 (Veizer 1983a, b; Land 1985). In dolomites, Na shows positive correlations with Mn ($r = 0.80$); and Mg ($r = 0.76$) (Fig. 5F), which indicate that the Na contents were enriched rather than decreased, perhaps due to the nature and interactions of the diagenetic fluids. Na is mostly below the detection limit (BDL) in HCMs and subsequently enriched during diagenesis.

Recrystallization

An increase in crystal size and non-planar texture are considered petrographic characteristics of the recrystallized dolomites (Kupecz and Land 1994; Machel 2004). These are evident in all the dolomite phases (P2, P3 and P5 dolomites). Despite that ancient dolomites are expected to exhibit ordered configuration, the older and recrystallized dolomites exhibit disordered configuration and/or early diagenetic conditions (e.g. Kupecz et al. 1993). This is seen in geochemical compositions among the studied P2 dolomites with a wider range of elemental compositions (Fig. 5A–F) and varied clusters signifying compositions of early and late diagenetic dolomites. The other dolomite groups, P3 and P5, show clustered distributions with elevated Mn and Mg contents but depleted Sr contents, implying late diagenetic dolomitization. The varied ordering in P2 dolomites could be explained by their exposure to varied diagenetic durations (Kupecz et al. 1993). This further implies that the P2 dolomites were initially subjected to the diagenetic environment in a relatively shorter period of time and later affected by diagenesis for a longer period where the remaining metastable phases underwent further stabilization resulting in the formation of late diagenetic dolomites. While the P3 and P5 dolomites were subjected to diagenesis sufficiently long period that stabilized the metastable dolomites and produced late diagenetic (recrystallized) dolomites. The recrystallization is clearly evident by the depletion of Sr and enrichment of Mn from the HCMs (e.g. Jacobsen and Kaufman 1999; Zhang et al. 2014).

Geochemical traits of the recrystallized dolomites include decreased REE, Sr, and Ba concentrations. The P2 dolomites from the earliest dolomitization phase have the widest range of $\sum$REE + Y values. These could have resulted from prevalent progressive/episodic stabilization of dolomites where higher values represent initial stabilization of early diagenetic dolomites while relatively lower values represent late-stage recrystallization. The P2, P3 and P5 dolomites have recorded the lower $\sum$REE + Y values, and imply that P2 dolomites, together with P3 and P5 dolomites have undergone more intense late-stage recrystallization. The Dolomites with higher Sr levels are interpreted as evidences of a lower degree of recrystallization while those with lower Sr levels are indicative of losing their original Sr during recrystallization. These phenomena are evident in P3–P5 and a few samples of P2 (Brand and Veizer 1980; Land 1980, 1985; Mazzullo 1992; Malone et al. 1996). The decrease in average Sr content from P2 (80.7 ppm) to P5 (39.8 ppm) suggests that the degree of recrystallization of the dolomites increased from P2 to P5. The relatively lower mean Sr contents in P3 (45.7 ppm) and P5 (39.8 ppm) dolomites indicate that these dolomites underwent late diagenesis and the highest degree of recrystallization. The wide range of Sr content in P2 dolomite, (32–203 ppm), reflects that these dolomites underwent both early and late diagenesis, suggesting that the P2 dolomites underwent various degrees of recrystallization.

Sr content decreases with increasing crystal size. Diagenetic dolomites have coarser crystals than primary, smaller dolomite crystal sizes, and may contain lesser Sr contents (Kupecz and Land 1994). This is in line with observations from petrographic studies revealing that the dolomites with larger dolomite crystals (partial P2, P3 and P5 dolomites) contain comparatively lower Sr content and P5 dolomites with largest crystals have the lowest Sr concentrations.

The studied samples are further analyzed using $(La/Sm)_{SN}$ vs $(La/Yb)_{SN}$ plot (Fig. 4C; Reynard et al. 1999) to interpret the prevalent dominant mechanisms (adsorption and/or substitution) during diagenesis. Relatively higher $(La/Yb)_{SN}$ ratios than seawater could be interpreted to be LREE enrichment contributed through the adsorption process at the sediment–water interface during post-depositional features such as early diagenesis (Reynard et al. 1999; Picard et al. 2002). According to Reynard et al. (1999), the $(La/Yb)_{SN}$ values < 2.5 indicate only a minor adsorption effect during early diagenesis. The $(La/Yb)_{SN}$ and $(La/Sm)_{SN}$ ratios are decreasing in selected dolomites and are parallel to the late diagenetic trend (Fig. 4C). Together, these observations suggest that the samples are affected by recrystallization (Reynard et al. 1999). The manifestation of corresponding decreased $(La/Yb)_{SN}$ and $(La/Sm)_{SN}$ ratios is often associated with MREE enrichment and shows "bell-shaped" REE distribution (Picard et al. 2002). However, such a trend is not recorded clearly though few samples show relative enrichment of MREEs, which can be related to Sm concentrations

in biogenic apatites with seawater-type patterns (e.g. Reynard et al. 1999).

Diagenetic fluids

As the incorporation of REEs into calcite is restricted by a relatively narrow range of partition coefficient values (Zhong and Mucci 1995), the changes shown by the REEs reflect the nature and intensity of crystallization processes, oceanic composition and/or characteristics of fluids that precipitated the carbonates (Azomani et al. 2013). Thus, they serve as proxies for the chemistry and the source of the fluids (Nothdurft et al. 2004) in which the mineral phases were precipitated. REE contents in the dolomites are controlled by several factors as follows| i.e. (a) the concentration of REE in the parental unaltered rocks, (b) the REE contents in the dolomitizing fluids, (c) the partitioning of REE between the dolomitizing fluids and dolomite and (d) fluid-rock ratios during diagenesis (Banner et al. 1988a, b; Qing and Mountjoy 1994). Unlike limestone, dolomite is uncommon to be used as an REE proxy to reconstruct the REE composition of the palaeo-seawater (Yamamoto et al. 2004). However, both ancient limestones and dolostones are used as proxies for the reconstruction of REE + Y compositions of ancient seawater that deposited the carbonates (e.g. Kamber and Webb 2001; Azmy et al. 2011).

The REE spectra of the dolomites and HCMs, the shale normalized REE patterns and concentrations show no systematic variations but look identical (e.g. Frimmel 2009). The overall relatively flat shapes of the REE patterns of the precursor limestones are often inherited and conserved in the dolomites. This reflects that the composition of the diagenetic dolomites is primarily controlled by the precursor carbonate and that fluids that formed the dolomites probably contained seawater that deposited the limestones (e.g. Azomani et al. 2013). However, the REEs of the HCMs are significantly controlled by the detrital input and thus show relatively flat PAAS normalized REE trends. In other words, it is construed that the extent of dolomitization and REE concentrations are unrelated. This interpretation is consistent with the findings of earlier studies that stated that the dolomitization and subsequent recrystallization do not significantly modify the general shape of the REE + Y patterns of the precursor carbonates (Banner et al. 1988a, b; Qing and Mountjoy 1994; Frimmel 2009; Wang et al., 2009; Allwood et al. 2010; Nagarajan et al. 2011; Zhao and Jones 2013; Liu et al. 2019; Smrzka et al. 2019. The REE concentrations of P2 dolomites (45.7 ppm) are only slightly higher than that of the HCMs (45.3 ppm) and show a decreasing trend from P2 to P5 dolomites. However, the REE patterns of different dolomite phases did not differ much, implying that the REEs behave in a similar way during dolomitization with no apparent fractionation although the REE amounts decreased during dolomitization process (Wang et al. 2009). This also implies low ratios of fluid to rock volumes (e.g. Banner et al. 1988a, b; Webb and Kamber 2000; Nothdurft et al. 2004). This is reflected in the localized dolomitization as shown in field evidence. It also points to a focused source of the diagenetic fluids, consistent with the focused outflow of hydrothermal diagenetic fluid origin (Warren 2000; Davies and Smith 2006; Ronchi et al. 2012b). In the present study, dolomitization is limited along the fracture and stratabound with a small amount of diagenetic fluids involved and low fluid–rock reactions which has not significantly affected the REE contents and patterns during dolomitization process.

Dolomitization would not alter the REE contents of precursor carbonates if it is mediated by seawater-like dolomitizing agents because the REE contents of seawater are very low relative to that of limestone (Banner et al. 1988b). The average $\sum$REE + Y values of the HCMs and early dolomites are similar (P1: avg. 45.29; P2: avg. = 45.72) while that of the later dolomite phases are relatively lower (P3: avg. = 36.93; P5: avg. = 30.33). Hence, despite the observed similar REE patterns, a relatively higher $\sum$REE + Y range of values of P2 dolomites and subsequent lower REE values in successive dolomites suggested that the dolomitizing fluids of the late-stage dolomites were not mediated by seawater nor seawater-like fluids. This is consistent with the phenomenon found elsewhere (e.g. Azmy et al. 2011) and suggests that the dolomitization might have been mediated by basinal brines. The unaltered seawater-like REE signatures in the Kinta carbonates are due to less extensive dolomitization where the extent of cation exchange with dolomitizing fluids was not sufficient to alter the REE signatures of the Kinta carbonates (e.g., Nothdurft et al. 2004). Subsequently, the REE patterns of the Kinta dolomites were preserved even though the dolomitization was not mediated by seawater or seawater-like fluids. The inference of dolomitization from basinal brines is in conformity with previous studies (Ramkumar et al. 2019) that espoused episodic dolomitization by tectono-thermal events; Xin Hui et al. (2021) that proposed local and limited availability of Mg^{2+} for dolomitization).

The mixing of seawater and hydrothermal fluids of unknown compositions would affect the REE pattern (Franchi et al. 2015; Zhao et al. 2018). The slight depletion of HREE in both calcite and dolomite relative to the LREE may suggest the involvement of hot brines but at different temperatures and burial settings (Azomani et al. 2013). Depletions of LREE and HREE result in enrichment of MREE. This is recognized as a "bell-shaped" pattern by Picard et al. (2002) and considered as a secondary feature that departs from seawater patterns (e.g. German and Elderfield 1990; Shields and Stille 2001; Shields and Webb 2004). In this regard, a binary diagram of $(La/Sm)_{SN}$ versus $(Gd/Yb)_{SN}$ is employed to ascertain the distribution pattern of REE. The studied samples mostly plotted (dolomites of P2,

P3) in the field "A": $(La/Sm)_{SN} < 1$, $(Gd/Yb)_{SN} > 1$, which indicates enrichment of MREE. Few HCMs (P1) fall in the field "B" and indicate enrichment of LREE (Fig. 4B). However, enrichment of MREE is relatively lesser and thus, insignificant alteration of the REEs during dolomitization could be inferred.

Positive Eu anomaly and light (LREE) to middle (MREE) REE-enrichment distributions are interpreted to be the resultant of high-temperature hydrothermal modification or reduced and acidic hydrothermal fluids (Bau and Dulski 1999; Bau et al. 2010; Delpomdor et al. 2013; Navarro-Ciurana et al. 2017). Hence, the positive Eu anomaly as observed in the HCMs and one sample each from P2 and P3 dolomites, coupled with overall association with minor MREE enrichment can be considered as influenced by hydrothermal activities (e.g. Delpomdor et al. 2013). This could be a product of either admixture of hydrothermal fluids or co-precipitation of hydrothermal Fe-sulphide (e.g. Frimmel 2009). The positive loadings of Si, Al, Cu with Eu anomaly of dolomites can explain the possibility of mixing heated brine water with seawater. In addition, Eu anomalies can occur as either positive or negative, varying with the redox state of the hydrothermal fluid and its total activity, where pyrite-bearing carbonate exhibits positive Eu anomaly and Fe-oxide rich domains show negative Eu anomaly (Fig. 6A) (Frimmel 2009). Eu anomalies can also be contributed by Eu mobilization by diagenetic fluids (Frimmel 2009). The presence of Eu^{2+} in the weathered source can lead to preferred leaching of Eu during weathering (Nozaki et al. 2000), particularly if it is feldspar enriched (Kamber et al. 2005). However, no feldspar is observed through petrographic and mineralogical studies. Thus, it is prudent to interpret that the Eu anomalies of the carbonates are not controlled by the feldspars. Also, there are no significant positive or negative correlations observed for Eu/Eu* with K/Al and Na/Al ratios, which unequivocally establish that the Eu anomaly is not controlled by the detrital feldspars (Fig. 6B, C) (e.g. Nagarajan et al. 2011).

The distinct positive Eu anomaly in the carbonates can represent an elevated Eh in the parent fluid (Lee et al. 2003) due to the increased Eu^{3+}/Eu^{2+}ratio. Slight positive or negative Eu anomalies in dolomites are suggested to be contributed by Eh alteration of parent fluid (Kučera et al. 2009). The primary fluid composition may also explain the positive Eu anomalies in carbonates (Kučera et al. 2009). Mobilization of Eu during high temperature (> 200 °C) diagenetic processes or metamorphism of rocks with Ca-plagioclase where Eu^{3+} is reduced to Eu^{2+} may cause positive Eu anomalies in fluids (e.g. Schwinn and Markl 2005). Eu^{2+} ions are easily remobilized in aquatic thermal solutions as they tend to adsorb on mineral surfaces and within the intergranular spaces after cooling (Kučera et al. 2009). This could explain the positive Eu anomalies in the HCMs. It is envisaged that hydrothermal alteration took place at elevated temperature during post-depositional times before initiation of dolomitization, contributing to most positive Eu anomalies found in HCMs but not dolomitized carbonates. According to Zhao et al. (2018), even 0.2% of high-temperature fluids in the seawater can display a positive Eu anomaly. Based on this surmise, it can be envisaged that even 0.1% hydrothermal high-temperature fluid may account for the observed Eu anomalies in HCMs (Fig. 6D, E). Although the positive Eu anomaly in dolomites could be interpreted due to the dilution of hydrothermal fluid with a large volume of ambient seawater (Bau et al. 2010; Johannessen et al. 2017; Zhao et al. 2018), the involvement of only a small volume of diagenetic fluids in the episodic localized dolomitization obviates this interpretation. The REE + Y abundances in hydrothermal fluids are of negligible importance for resulting REE + Y patterns of dolomites (Kučera et al. 2009). This explains the absence of anticipated positive Eu anomalies and elevated REE contents in dolomites despite their hydrothermal alteration.

Kučera et al. (2009) suggested that fluid temperature may have a great influence on the fluid–rock interaction and total REE concentrations. The dolomites precipitated from fluids of higher temperature are mostly REE-enriched than those of colder fluids, which are mostly REE-depleted. This phenomenon due to the leaching of REE-bearing minerals (e.g. monazite, allanite) in higher temperatures may result in higher total REE + Y content (Kučera et al. 2009). The explanation of relatively higher total REE concentration in the HCMs due to elevated temperatures is consistent with the presence of positive Eu anomalies in the same group, which can be attributed to prevalent high temperatures. The relatively depleted REE contents in successive dolomites can be related to the recrystallization or the REE remobilization of dolomite (Elderfield and Sholkovitz 1987; Kučera et al. 2009; Smrzka et al. 2019), at an even higher temperature. Applying these to the studied samples, the latter dolomite phases can be deemed to be formed at higher temperatures as evident in larger crystal sizes but they have relatively lesser REE concentrations. The absence of prominent positive Eu anomalies in studied dolomites, coupled with the relatively depleted REE concentrations compared to the HCM, suggests dolomitizing fluids with depleted REE contents. On the other hand, pH modifications in the solution can be a comparatively more important factor (Kučera et al. 2009). The REE contents in a solution increase with decreasing pH in different hydrothermal systems (Michard 1989). However, the total REE concentrations in dolomite samples do not show a significant correlation with either Sr or Na (salinity indicators). These geochemical behaviors of the studied samples are anticipated due to previous studies (Ramkumar et al.2019; Xin Hui et al. 2021) and

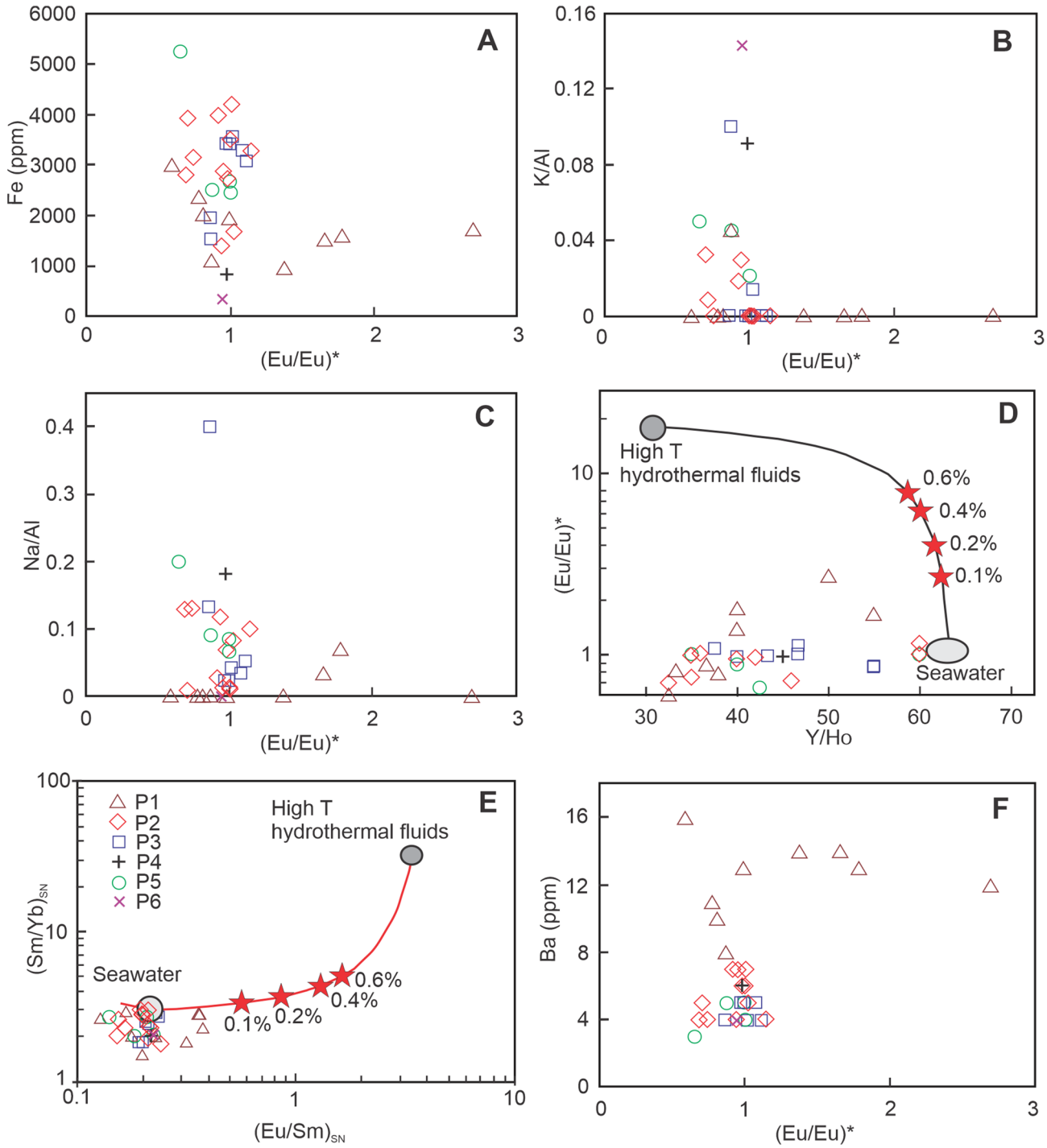

Fig. 6 **A**–**C** Eu/Eu* vs trace elements and its ratio explain the variation of Eu/Eu* which is not controlled by the detrital feldspars. **D** Y/Ho Vs. Eu/Eu* plot indicates at least 0.2% of High-T hydrothermal (> 350 °C, Fluid contributions). **E** The Eu/Sm vs Sm/Yb plot shows a little lesser contribution of hydrothermal fluid (after Zhao et al. 2018). **F** Ba Vs. Eu/Eu* plot shows no definite trend amongst the Kinta carbonates

field and petrographic observations where occurrences of hydrothermal alteration are reported. These studies interpreted that the fluids originated from the underlying rocks, channeled up-dip through the fractured system, and dolomitized the HCMs of the Kinta Valley.

Fe and Mn contents in dolomite serve as useful indicators as they reflect both the redox conditions during

dolomitization and the availability of these elements in the dolomitizing fluids (Budd 1997). The dolomites formed in normal marine environments commonly contain low Fe and Mn concentrations varying from 3 to 50 ppm and 1 ppm, respectively (Veizer 1983b), although the different ranges of higher values have also been reported (Vahrenkamp and Swart 1990; Budd 1997). Significantly higher concentrations of Fe may imply the possibility of diagenetic fluids related to magmatic activities (e.g., Hou et al. 2016) or circulated through volcanic rocks, whereas Mn concentrations could reach up to 34,000 ppm in carbonate diagenesis involving meteoric waters (Driese and Mora 1993). Mn concentrations higher than 400 ppm are considered as a common feature implying non-marine fluids (Bruckschen et al. 1999). The Fe and Mn contents in the Kinta dolomites (1399–5246 and 1371–2649 ppm, respectively) are significantly higher than the marine dolomites and much lower than the carbonates that underwent diagenesis under meteoric water. Elevated Fe and Mn levels in the dolomites by substituting for Mg imply that the dolomitization occurred under reducing conditions (Land 1986). This inference warrants dolomitization at deeper burial conditions (Adabi and Mehmandosti 2008). The source of the Fe and Mn in dolomitizing fluids must be a non-carbonate, for instance, associated siliciclastics or underlying crystalline basement (Vandeginste et al. 2013), which is an important source of magnesium. The range of Fe contents in the dolomites resembles those of dolomites precipitated from hot, saline, basinal fluids as reported by Aharon et al. (1987) on the atolls at Niue, South Pacific (620–5740 ppm). The dolomites enriched in calcium (30.4–43.5 mol % CaO) and iron (1398.9–5245.7 ppm) are typical characteristics of phases that precipitated from basinal fluids rich in Ca and Fe (Amthor and Friedman 1992). In addition, the medium to coarse crystalline dolomites are likely to be derived from compaction of shales on the underneath, and the basinal brines. The released Mg^{2+} from shale may have migrated upwards through pore fluids and dolomitized the overlying carbonates along the fracture and bedding plane. Fe and Mn concentrations in the studied dolomites show no correlation between them ($r = -0.03$), which could be explained by the progressive enrichment of Mn content in fluids due to disequilibrium (Lonne and Al-Aasm 2000).

Sr concentrations in the dolomites may reflect the nature of the dolomitizing fluids (e.g., Lu and Meyers 1998). The Dolomites precipitated from normal seawater should have a theoretical equilibrium concentration of 470–550 ppm Sr with reference to the dolomite–water distribution coefficient (Veizer 1983b) (Table 2). Conversely, "pene-contemporaneous" dolomites formed in evaporitic settings contain about 500–700 ppm (Land 1991) and fluids of high salinity origin from hypersaline sabkhas have low Sr contents (< 550 ppm) (Tucker and Wright 1990). The Sr concentrations of the dolomite samples (31–203 ppm) are significantly lower and imply that these dolomites were not precipitated from normal marine, evaporitic settings and hypersaline sabkhas. The low Sr levels recorded in the studied dolomites are comparable with those precipitated from basinal brines, which are Sr-depleted fluids (e.g. Sperber et al. 1984; Azmy et al. 2011; Azomani et al. 2013; Hou et al. 2016) (Table 2). Although low Sr contents may also associate with Sr-depleted meteoric water fluids (Pierson 1981), this is most unlikely to be the case as the dolomite bodies are associated with structure-controlled geobodies with closed fractures indicative of fluids coming from beneath. Dolomitizing fluids expelled from clastic rocks or evaporates are attributed to low Sr concentrations (Huang et al. 2006). Accordingly, in addition to the inferences based on geochemistry and lithology, the emanation of dolomitizing fluids from the underlying carbonaceous–argillaceous Ordovician strata seems to be plausible.

Sodium, being the most abundant cation in the seawater, is recognized as a useful palaeosalinity tracer in ancient fluids and carbonates (Land and Hoops 1973; Veizer et al. 1977; Sass and Bein 1988). Hence Na can also be a potential indicator of the salinity of the dolomitizing fluids (Budd

Table 2 Comparison of elemental compositions (ppm) in carbonates formed from various sources

Source/element	[a]Seawater calcite	[b]Seawater dolomite	[c]Present study ($n = 33$)	[d]Hot basinal fluid	[e]Modified seawater	[f]Hydrothermal fuids
Sr	1000	470–550	31–203	18–155	80.5–886.4	BDL-2489
Na	200–300	110–160	74.2–296.7	–	22.3–712.3	BDL-349
Fe	2–39	3–50	1399–5246	276–24,955	BDL to 4441.1	BDL to 44,886
Mn	1	1	1371–2649	22–6049	5.2–28.0	BDL-1216
Ba	0.2–0.8	0.1–0.5	3–7	–	–	BDL to 4907

[a,b]Veizer (1983b)

[c]Present study

[d]Hou et al. (2016)

[e]Li et al. (2015)

[f]Zhang et al. (2009)

1997). High contents of Na in all the dolomites indicate that they were formed from higher salinity non-marine dolomitizing fluids (Kirmaci 2008; Azomani et al. 2013) (Table 2). However, interpreting the concentrations of Na is tricky and should be used with caution, as Na enrichment in dolomite can be due to solid and fluid inclusions of NaCl, Na substitution in the crystal lattice (Qing and Mountjoy 1989), and contamination by Na-bearing clay minerals and tuffites (Kirmaci and Akdag 2005; Kirmaci 2008). In the present study, a close relationship of Na with Mn and Mg indicates that the effect of diagenetic fluids increased the Na content in dolomite. This inference is contrary to the common occurrence that the contents of Na may be lowered during an increased degree of recrystallization. Seawater typically contains Ba contents of 0.01–0.05 ppm, while subsurface brines commonly range from 1 to nearly 6000 ppm Ba (Hanor 1979) (Table 2). The Ba content of the Kinta dolomites in the range of 3–7 ppm (Fig. 6F) again reaffirms the non-marine origin of the dolomites. Hence, inference of non-marine origin of the diagenetic fluids is justifiable. He et al. (2006) reported that Ba can be incorporated into the dolomite lattice only at high temperatures. Thus, the higher than normal seawater Ba content in the studied dolomites reflects a hydrothermal fluid setting; again pointing to a basinal brine origin for the dolomitizing fluids.

Occurrences of various dolomite phases as evident from field, petrography and geochemistry findings reflect multiple dolomitization episodes although geochemically insignificant variations are shown among the phases. Together, they point towards the contribution of episodic fluxes. The similar REE profiles of the various dolomite phases and HCMs with insignificant differences among them imply that the various dolomite generations are formed by diagenetic fluids of identical composition (e.g. circulated basinal brines) but at different temperatures and burial environments (e.g. Azomani et al. 2013).

P1 Diagenetic fluids The first phase of fluid flux and alteration of the geochemical composition of the host phases by the hydrothermal fluids is evident from the presence of positive Eu anomalies, and lower contents of Fe, and Mn, and higher contents of Sr and Ba. The geochemical traits exhibited in limestone samples generally point towards a non-marine origin of the diagenetic fluid. Influences of hydrothermal fluid that emanated from subsurface are affirmed by the positive Eu anomalies (Bau and Dulski 1999; Frimmel 2009) and high Ba values (He et al. 2006). The highest positive Eu anomalies and Ba values as shown in the P1 carbonates reflect the involvement of the highest temperature during diagenesis.

P2–P5 Diagenetic fluids The diagenetic fluids of the dolomites (P2–P5) exhibit similar features namely, low Sr/Ca ratios, lower positive Eu anomalies, higher Mn, Fe (Fig. 6E) and Na and lower Sr and Ba contents. However, the ∑REEs varied from P2–P5, showing a declining trend. These features strongly support that the fluids are basinal brines that are mixed with seawater derived from underneath. The fluids have dissolved and dolomitized the HCMs along the fractures under high temperatures. High Fe and Mn values reflect the reducing nature of the diagenetic fluids (Land 1986; Warren 2000) and Sr depletion implying the source of diagenetic fluids to be hot, reducing, basinal fluids (Azmy et al. 2011; Azomani et al. 2013; Hou et al. 2016).

The relatively lower concentrations of Fe and Mn in some of the P2 dolomites imply a less reducing diagenetic environment with a lower supply of divalent Fe and Mn (e.g. Qing and Mountjoy 1989). The reducing conditions of P2 dolomites are further supported by illustrations from the plot of Sr/Ca ratio vs Mn (Fig. 5B). The presence of anhedral dolomite crystals, depletion of positive Eu anomalies and Sr contents imply relatively higher temperature during diagenesis where high temperatures facilitated remobilization of Eu resulting in depleting positive Eu anomaly (Kučera et al. 2009) and lower Sr values indicate a higher degree of recrystallization (Brand and Veizer 1980; Land 1980; Mazullo 1992). The higher Mn contents of P2–P3 dolomites despite decreasing trend of Fe contents could be attributed to preferential incorporation of Mn^{2+} with decreasing Eh due to higher solubility of Mn^{2+} than Fe^{2+} over a larger range of Eh conditions (Harris et al. 1985) and higher partition coefficient of Mn (5–30) comparable to that of Fe (1–20) in substitution for Ca and/or Mg in dolomite (James and Jones 2015). This resulted in availability of Mn^{2+} ions for incorporation into dolomite lattice when Fe was not readily available and or actively substituted. Both Fe and Mn ions are actively incorporated into calcite and dolomite under ideal reducing conditions (Lonne and Al-Aasm 2000). Hence, the lower average Fe contents in P3 dolomites could indicate a reducing condition of the fluids that were not sufficient/significant enough to liberate more Fe ions for incorporation into dolomite. Although the decreasing trend in Fe values was observed in the P2–P3 dolomites, the Mn contents showed a decrease in the P2–P3 dolomites. The Fe and Mn values generally overlap in the dolomite phases and denote similar fluid chemistry from similar sources. The manifestation of larger anhedral dolomites crystals with non-planar texture and saddle dolomite (largest crystal), coupled with lesser positive Eu anomalies and significantly depleted Sr concentrations in P5 dolomites indicates another fluid flux with relatively higher temperature. This inference is comparable to the study of Al-Aasm (2003).

Paragenesis and implications for tectonic and thermal events

Integration of the geochemical signatures of individual facies types (Table 1) with field and petrographic characteristics suggests an intrinsic relationship to prevalent tectono-thermal events. Increasing trend of Mn values coupled with decreasing trends of ∑REE, Sr and less positive Eu anomalies reflect incremental changes of thermal conditions during formations of various phases of dolomites set in this general backdrop, the first episode of the diagenetic history of the studied Kinta carbonates was manifested by a positive Eu anomaly in the HCM produced by diagenetic modification in a hydrothermal setting (Bau and Dulski 1999; Frimmel 2009). This event occurred prior to the onset of the dolomitizations resultant from successive thermo-tectonic events. This high-temperature diagenetic event was associated with a distant submarine Permian volcanic event near Central Range (Basori et al. 2017) that supplied hydrothermal fluids hot enough to alter REE signatures into positive Eu anomaly (Bau and Dulski 1999; Frimmel 2009; He et al. 2006).

The younger dolomitization events in burial conditions are reflected in petrographic evidences such as dolomite crystals along the dissolution seams and field evidences of dolomite geobodies that are enclosed within inverted "v" fractures that terminated below surface level. The inferred compaction event is further supported by the occurrences of low-amplitude stylolites in the HCMs (P1). These low-amplitude stylolites may have been formed at a burial depth of at least 500 m (Duggan et al. 2001; Kirmaci 2008). The prevalence of dolomitization events in subsurface conditions is further supported by the occurrences of medium to coarse crystalline fabrics (e.g. Azomani et al. 2013). This is consistent with the occurrences of dolomites along the dissolution seams that resulted from compaction events implying precedence of compaction before the dolomitization event. The comparatively higher Fe and Mn contents of HCMs (least dolomitized) also support the inference of subsurface, reducing conditions of dolomitization (Land 1986; Warren 2000). The first dolomitization event could be associated with the folding and faulting prevalent during the Permo-Triassic Sibumasu-East Malaya collision (Ramkumar et al. 2019; Xin Hui et al. 2021). The presence of positive Eu anomalies and highest Ba values indicate the involvement of diagenetic fluids of high temperature (Bau and Dulski 1999; Frimmel 2009; He et al. 2006). This dolomitizing fluid might have penetrated through fractures and then permeable beds. This inference implies high pressure (compactional?) for allowing the channeling of the dolomitizing fluid. The diagenetic system was increasingly open as reflected by decreased Sr contents (Brand and Veizer 1980) contributed by micro faults, fractures and stylolites formed during the episodic tectonic event (Ramkumar et al. 2019; Xin Hui et al. 2021).

The HCMs were subjected to subsequent dolomitization events during succeeding thermo-tectonic events. Brecciated HCM with fractures filled with replacement dolomites represents the initiation of second phase tectonic event related to post-orogenic phase of subsidence that resulted in the formation of collapse breccias. The subsequent dolomitization is recognized in the field by distinctive varied color and dolomite petrographic textures. The medium to coarse crystalline fabric of the dolomites, and their increasing crystal size reflect the replacement dolomitization events associated with enhanced temperature and pressure (Warren 2000) and deep burial conditions (e.g. Azomani et al. 2013). This dolomite phase recorded increased Fe and Mn contents but depleted Eu anomalies implying higher temperature of diagenetic fluids that enabled the remobilization of Fe, Mn and Eu contents (e.g., Kučera et al. 2009). Though non-stoichiometric calcian dolomite in P2 dolomites is interpreted to have been formed under a relatively closed diagenetic system, it may not have been a perfect closed system. The depletion in Sr values signifies an open system (Brand and Veizer 1980) with increased pathways (fractures) resultant from fractures formed during the tectonic event (Lonne and Al-Aasm 2000) and however, restricted fluid flow and/or Mg^{2+} supply (Azomani et al. 2013). This series of diagenetic events could be correlated with Late Triassic to Early Jurassic regional post-orogenic subsidence (Meng et al. 2021) and associated metamorphism.

The next dolomitization event is manifested in varied colored dolomite geobody with distinct sugary texture. The occurrence of sucrosic texture of the dolomites points towards a restricted fluid flow of dolomitizing fluids (Warren 2000) although depleted Sr contents are indicative of an increasingly open dolomitization system (Brand and Veizer 1980). The increase in openness of the system could be explained by the introduction of external dolomitizing fluids through fractures and fluid flow through them. However, overlapping of most elemental compositions among the dolomite phases implies similar P–T ranges during multiple dolomitization events. The overlapping geochemical compositions also indicate dolomitization by fluids of identical composition in a closed diagenetic system at varying temperatures (Azmy et al. 2011; Azomani et al. 2013; Mahboubi et al. 2016) or burial fluids of the same origin that have circulated in a closed to semi-closed system (Azomani et al. 2013). A relatively higher temperature is also reflected through higher positive Eu anomalies and Fe and Mn range. The thermo-tectonic event that could be correlated with the similar P–T ranges but a higher temperature could be the Late Cretaceous fracturing event with the formation of NW–SE and NE-SW faults and associated regional thermal anomaly that produced acidic dykes that filled the fractures and Main Range pluton edges (Sautter et al. 2017).

The next dolomitization phase is evident in yet another different colored dolomite geobody recognized in the field. Petrographically, it shows an increment in crystal size indicative of the association of higher temperature and pressure during the replacement dolomitization events (Warren 2000). Low porosity in these dolomites reflects a rich supply of magnesium-rich fluids that enabled pervasive dolomitization in an open system (e.g. Azomani et al. 2013). Nevertheless, the higher porosity as exhibited in late-stage dolomites suggests a closed to semi-closed system with a low water–rock ratio and limited supply of magnesium source, which has not been able to occlude the available and or newly created pore spaces completely. In addition, the absence of void-filling dolomites implies a limited external supply of Mg^{2+} ions and hence there was no extra dolomite to occlude the newly-developed inter-crystalline pore spaces. The increasing trend of Fe and Mn from P1–P5 dolomites implies an increase in reducing conditions from the early to late replacement dolomites (Azomani et al. 2013). The intensified tectonic events that contributed to this dolomitization phase could be the reactivation of major dextral slip faults during the Late Cretaceous to Paleogene associated with the early rifting stage across the Malay Peninsula. Despite the dolomite phases showing an increasingly open diagenetic system, occurrences of mm-thick calcite veins cutting through all dolomite phases and thermogenic calcite in the last phase of diagenetic history imply a closed diagenetic system with a limited external supply of Mg^{2+} ions. This is in line with the thermal event during quiescence of tectonics during the Late Cenozoic Period where no fractures were created to provide fresh sources of diagenetic fluids and Mg^{2+} ions, hence diagenetic system remained closed.

Conclusions

The Kinta carbonates were deposited under open marine oxygenated waters. The marine signature of the studied carbonates is affirmed by the REE + Y patterns. Prevalence of multiple episodes of physical and chemical compaction, fracturing, dolomitization and recrystallization are inferred from seven facies types which in turn are grouped into two distinct clusters representative of early and late diagenetic events. These clusters have unique signatures of trace and rare earth elements such as elevated $\sum$REE + Y, Fe, Mn, Na and Ba contents, depleted Sr concentrations, minor MREE enrichment and positive Eu anomalies. Prevalent changes in the P–T conditions have imprinted variable diagenetic signatures in terms of fluid chemistry of diagenetic fluid chemistry, openness of the diagenetic system and intensity of water–rock interaction. Absence of pervasive diagenetic transformation and occurrences of diagenetic changes only along the interfaces wherein the circulating fluids and host rocks interacted, which in turn were facilitated by the multiple fractures that originated by the tectono-thermal events of Permian to Cretaceous are also inferred by the present study. The temporal evolution of the diagenetic fluids was characterized by the presence of positive Eu anomaly in P1 limestone but depleting in dolomites, low Fe, Mn but high Sr, Ba values in P1 limestone while high Mn, Fe, Na but low Sr and Ba contents in dolomites, decreasing REE values from P2–P5 dolomites. The thermal event during tectonic quiescence had played primary and secondary roles in multi-stage diagenetic events by providing connectivity enabling fluid flow and producing multiple fluxes of diagenetic fluid as deep-circulating crustal hydrothermal fluids. The diagenetic fluids show affinity to basinal brines that emanated from tectono-thermal compaction of underlying Ordovician carbonaceous-argillaceous strata. The updip movement of fluids was facilitated by fractures and bedding planes, the thermal events have produced episodic crystallization/replacement of dolomite phases, that culminated in precipitation of calcite as the final event when the limited availability of Mg^{2+} was exhausted.

Supplementary Information The online version contains supplementary material available at https://doi.org/10.1007/s13146-022-00802-4.

Acknowledgements The anonymous reviewers and the editor are thanked for constructive criticisms and suggestions that helped the authors to improve the manuscript significantly. Financial assistance for fieldwork by MR and PX was supported by a Shell Grant from the South East Asia Carbonate Research Laboratory, Universiti Teknologi Petronas, Malaysia. The authors thank Lafarge for allowing the outcrop study at the quarry. This work benefitted from the financial support from Curtin University Malaysia through the Curtin Malaysia Strategic Research fund (RN) for analyses of whole-rock geochemistry. PX thanks UTP for providing a Research scholarship that enabled the conducting of part of this work.

Funding Open Access funding enabled and organized by CAUL and its Member Institutions. Universiti Teknologi Petronas, Curtin Malaysia.

Open Access This article is licensed under a Creative Commons Attribution 4.0 International License, which permits use, sharing, adaptation, distribution and reproduction in any medium or format, as long as you give appropriate credit to the original author(s) and the source, provide a link to the Creative Commons licence, and indicate if changes were made. The images or other third party material in this article are included in the article's Creative Commons licence, unless indicated otherwise in a credit line to the material. If material is not included in the article's Creative Commons licence and your intended use is not permitted by statutory regulation or exceeds the permitted use, you will need to obtain permission directly from the copyright holder. To view a copy of this licence, visit http://creativecommons.org/licenses/by/4.0/.

References

Adabi MH, Mehmandosti AE (2008) Microfacies and geochemistry of the ilam formation in the Tang-E-Rashid area, Izeh, S.W. Iran.

J Asian Earth Sci 33:267–277. https://doi.org/10.1016/j.jseaes.2008.01.002

Adams AE, Mackenzie WS, Guilford C (1984) Atlas of sedimentary rocks under the microscope. Longman, Harlow

Aharon P, Socki RA, Chan L (1987) Dolomitization of atolls by sea water convection flow: test of a hypothesis at Niue. South Pacific J Geol 95(2):187–203

Al-Aasm IS (2003) Origin and characterization of hydrothermal dolomite in the Western Canada sedimentary basin. J Geochem Explor 78–79:9–15. https://doi.org/10.1016/S0375-6742(03)00089-X

Alibo DS, Nozaki Y (1999) Rare earth elements in seawater: particle association, shale-normalization and Ce oxidation. Geochim Cosmochim Acta 63:363–372. https://doi.org/10.1016/S0016-7037(98)00279-8

Allwood AC, Kamber BS, Walter MR, Burch IW, Kanik I (2010) Trace elements record depositional history of an early Archean stromatolitic carbonate platform. Chem Geol 270:148–163. https://doi.org/10.1016/j.chemgeo.2009.11.013

Amakawa H, Alibo DS, Nozaki Y (2000) Nd isotopic composition and REE pattern in the surface waters of the eastern Indian Ocean and its adjacent seas. Geochem Cosmochim Acta 64(10):1715–1727. https://doi.org/10.1016/S0016-7037(00)00333-1

Amthor JE, Friedman GM (1992) Early- to late-diagenetic dolomitization of platform carbonates: lower Ordovician Ellenburger Group, Permian Basin, West Texas. J Sediment Petrol 62(1):131–144. https://doi.org/10.1306/D42678AC-2B26-11D7-8648000102C1865D

Anan T, Wanas H (2015) Dolomitization in the carbonate rocks of the upper Turonian Wata formation, West Sinai, NE Eygpt: petrographic and geochemical constraints. J Afr Earth Sci 111:127–137. https://doi.org/10.1016/j.jafrearsci.2015.07.015

Azmy K, Brand U, Sylvester P, Gleeson SA, Logan A, Bitner MA (2011) Biogenic and abiogenic low-Mg calcite (bLMC and aLMC): evaluation of seawater-REE composition, water masses and carbonate diagenesis. Chem Geol 280:180–190. https://doi.org/10.1016/j.chemgeo.2010.11.007

Azomani E, Azmy K, Blamey N, Brand U, Al-Aasm I (2013) Origin of Lower Ordovician dolomites in eastern Laurentia: controls and implications from geochemistry. Mar Petrol Geol 40:99–114. https://doi.org/10.1016/j.marpetgeo.2012.10.007

Banner JL, Hanson GN, Meyers WJ (1988a) Water-rock interaction history of regionally extensive dolomites of the Burlington-Keokuk Formation (Mississippian): isotopic evidence. In: Shukla V, Baker P (eds) Sedimentology and geochemistry of dolostones. SEPM, Tulsa, pp 97–114. https://doi.org/10.2110/pec.88.43.0097

Banner JL, Hanson GN, Meyers WJ (1988b) Rare earth element and Nd isotopic variations in regionally extensive dolomites from the Burlington-Keokuk Formation (Mississippian); implications for REE mobility during carbonate diagenesis. J Sediment Petrol 58(3):415–432. https://doi.org/10.1306/212F8DAA-2B24-11D7-8648000102C1865D

Bartley JK, Semikhatov MA, Kaufman AJ, Knoll AH, Pope MC, Jacobsen SB (2001) Global events across the Mesoproterozoic-Neoproterozoic boundary: C and Sr isotopic evidence from Siberia. Precambrian Res 111:165–202. https://doi.org/10.1016/S0301-9268(01)00160-7

Basori MBI, Zaw K, Meffre S, Large RR, Wan Hassan WF (2017) Pb-isotope compositions of the Tasik Chini volcanic-hosted massive sulfide deposit, Central Belt of Peninsular Malaysia: Implication for source region and tectonic setting. Island Arc 26(2):e12177. https://doi.org/10.1111/iar.12177

Bau M (1996) Controls on fractionation of isovalent trace elements in magmatic and aqueous systems: evidence from Y/Ho, Zr/Hf, and lanthanide tetrad effect. Contrib Mineral Petrol 123:323–333. https://doi.org/10.1007/s004100050159

Bau M, Dulski P (1996) Distribution of Yttrium and rare-earth elements in the Penge and Kuruman iron-formations, Transvaal Supergroup, South Africa. Precambrian Res 79:37–55. https://doi.org/10.1016/0301-9268(95)00087-9

Bau M, Dulski P (1999) Comparing yttrium and rare earths in hydrothermal fluids from the Mid-Atlantic Ridge: implications for Y and REE behaviour during near-vent mixing and for the Y/Ho ratio of Proterozoic seawater. Chem Geol 155:77–90. https://doi.org/10.1016/S0009-2541(98)00142-9

Bau M, Möller P, Dulski P (1997) Yttrium and lanthanides in eastern Mediterranean seawater and their fractionation during redox-cycling. Mar Chem 56:123–131. https://doi.org/10.1016/S0304-4203(96)00091-6

Bau M, Balan S, Schmidt K, Koschinsky A (2010) Rare earth elements in mussel shells of the Mytilidae family as tracers for hidden and fossil high-temperature hydrothermal systems. Earth Planet Sci Lett 299(3–4):310–316. https://doi.org/10.1016/j.epsl.2010.09.011

Braithwaite CJR, Rizzi G, Darke G (2004) The geometry and petrogenesis of dolomite hydrocarbon reservoirs. Geol Soc Lond, Special Publ 235:1–6. https://doi.org/10.1144/GSL.SP.2004.235.01.01

Brand U, Veizer J (1980) Chemical diagenesis of a multi-component carbonate system. I. Trace elements. J Sediment Res 50(4):1219–1236. https://doi.org/10.1306/212F7BB7-2B24-11D7-8648000102C1865D

Budd DA (1997) Cenozoic dolomites of carbonate islands: their attributes and origin. Earth-Sci Rev 42(1–2):1–47. https://doi.org/10.1016/S0012-8252(96)00051-7

Bruckschen P, Oesmann S, Veizer J (1999) Isotope stratigraphy of the European carboniferous: proxy signals for ocean chemistry, climate and tectonics. Chem Geol 161(1–3):127–163. https://doi.org/10.1016/S0009-2541(99)00084-4

Carr DD, Rooney LF, Freas RC (1994) Limestone and dolomite. In: Carr DD (ed) Industrial minerals and rocks, 6th edn. Society for Mining, Metallurgy and Exploration, Littleton, Colorado, pp 605–629

Chai L, Navrotsky A, Reeder RJ (1995) Energetics of calcium-rich dolomite. Geochim Cosmochim Acta 59(5):939–944. https://doi.org/10.1016/0016-7037(95)00011-9

Chen D, Qing H, Yang C (2004) Multistage hydrothermal dolomites in the Middle Devonian (Givetian) carbonates from the Guilin area. South China Sedimentol 51(5):1029–1051. https://doi.org/10.1111/j.1365-3091.2004.00659.x

Chen Y, Zhou X, Yang H (2010) Geochemical research and genesis of dolostones with different crystal characteristics occurring in the Upper Cambrian, central area of Tarim basin. Acta Sedimentol Sin 28(2):209–218 (**[in Chinese with English abstract]**)

Cicero AD, Lohmann KC (2001) Sr/Mg variation during rock-water interaction: implications for secular changes in the elemental chemistry of ancient seawater. Geochim Cosmochim Acta 65(5):741–761. https://doi.org/10.1016/S0016-7037(00)00594-9

Clements B, Burgess PM, Hall R, Cottam MA (2011) Subsidence and uplift by slab-related mantle dynamics, a driving mechanism for the Cretaceous and Cenozoic evolution of continental SE Asia? In: Hall R, Cottam MA, Wilson MEJ (eds) The SE Asian gateway: history and tectonics of the Australia-Asia collision. Geol Soc London Special Publications, London, pp 37–51. https://doi.org/10.1144/SP355.3

Cottam MA, Hall R, Ghani AA (2013) Late Cretaceous and Cenozoic tectonics of the Malay Peninsula constrained by thermochronology. J Asian Earth Sci 76:241–257. https://doi.org/10.1016/j.jseaes.2013.04.029

Davies GR, Smith LB (2006) Structurally controlled hydrothermal dolomite reservoir facies: an overview. AAPG Bull 90(11):1641–1690. https://doi.org/10.1306/05220605164

Delpomdor F, Blanpied C, Virgone A, Preat A (2013) Paleoenvironments in Meso-Neoproterozoic carbonates of the Mbuji-Mayi supergroup (Democratic Republic of Congo) –Microfacies analysis combined with C-O–Sr isotopes, major-trace elements and REE + Y distributions. J Afr Earth Sci 88:72–100

Dickson J (1965) A modified staining technique for carbonates in thin section. Nature 205:587. https://doi.org/10.1038/205587a0

Driese SG, Mora CL (1993) Physico-chemical environment of pedogenic carbonate formation in Devonian vertic palaeosols, central Appalachians, USA. Sedimentology 40:199–216. https://doi.org/10.1111/j.1365-3091.1993.tb01761.x

Duggan JP, Mountjoy EW, Stasiuk LD (2001) Fault-controlled dolomitization at Swan Hills Simonette oil field (Devonian), deep basin west-central Alberta. Can Sedimentol 48(2):301–323. https://doi.org/10.1046/j.1365-3091.2001.00364.x

Dutt A, Singh AK, Oinam G, Srivantava SK (2021) Depositional environment and tectonic backdrop of meta-carbonates in the Eastern Himalayan ophiolites, India: insights from calcite microstructures, whole-rock elements and stable isotopes. Carb Evap 36:34. https://doi.org/10.1007/s13146-021-00704-x

Elderfield H, Greaves MJ (1982) The rare earth elements in seawater. Nature 296:214–219. https://doi.org/10.1038/296214a0

Elderfield H, Sholkovitz ER (1987) Rare earth elements in the pore waters of reducing nearshore sediments. Earth Planet Sci Lett 82(3–4):280–288. https://doi.org/10.1016/0012-821X(87)90202-0

Escorcia LC, Gomez-Rivas E, Daniele L, Corbella M (2013) Dedolomitization and reservoir quality: insights from reactive transport modelling. Geofluids 13:221–231. https://doi.org/10.1111/gfl.12023

Folk RL (1974) Petrology of sedimentary rocks. Hemphill Publication Company, Austin, Texas

Fontaine H, Ibrahim BA (1995) Biostratigraphy of the Kinta Valley. Perak Geol Soc Malaysia Bull 38:159–172

Franchi F, Hofmann A, Cavalazzi B, Wilson A, Barbieri R (2015) Differentiating marine vs hydrothermal processes in Devonian carbonate mounds using rare earth elements (Kess Kess mounds, Anti-Atlas, Morocco). Chem Geol 409:69–86. https://doi.org/10.1016/j.chemgeo.2015.05.006

François T, Md Ali MA, Matenco L, Ng TF, Taib NI, Shuib MK (2017) Late Cretaceous extension and exhumation of the Stong and Taku magmatic and metamorphic complexes, NE Peninsular Malaysia. J Asian Earth Sci 143:296–314. https://doi.org/10.1016/j.jseaes.2017.04.009

Friedman GM (1965) Terminology of crystallization textures and fabrics in sedimentary rocks. J Sediment Petrol 35(3):643–655. https://doi.org/10.1306/74D7131B-2B21-11D7-8648000102C1865D

Frimmel HE (2009) Trace element distribution in Neoproterozoic carbonates as palaeoenvironmental indicator. Chem Geol 258:338–353. https://doi.org/10.1016/j.chemgeo.2008.10.033

Ganai JA, Rashid SA, Romshoo SA (2018) Evaluation of terrigenous input, diagenetic alteration and depositional conditions of lower carboniferous carbonates of Tethys Himalaya, India. Solid Earth Sci 3:33–49. https://doi.org/10.1016/j.sesci.2018.03.002

Gebretsadik HT, Sum CW, Yuriy GA, Hunter AW, Talib JAB, Kassa S (2017) Higher-resolution biostratigraphy for the Kinta Limestone and an implication for continuous sedimentation in the Paleo-Tethys, Western Belt of Peninsular Malaysia. Turkish J Earth Sci 26:377–394. https://doi.org/10.3906/yer-1612-29

German CR, Elderfield H (1990) Application of the Ce anomaly as a paleoredox indicator: the ground rules. Paleoceanography 5(5):823–833. https://doi.org/10.1029/PA005i005p00823

Ghani AA, Searle M, Robb L, Chung SL (2013) Transitional I-S type characteristic in the Main Range Granite, Peninsular Malaysia. J Asian Earth Sci 76:225–240. https://doi.org/10.1016/j.jseaes.2013.05.013

Gregg JM, Sibley DF (1984) Epigenetic dolomitization and the origin of xenotopic dolomite texture. J Sediment Petrol 54(3):908–931. https://doi.org/10.1306/212F8535-2B24-11D7-8648000102C1865D

Guruaribam V, Singh YR, Singh AK (2021) Age and depositional environment of carbonate exotics associated with the Disang group of Assam-Arakan Basin, Northeast India: constraints from microfossils and geochemistry. Carb Evap 36:46. https://doi.org/10.1007/s13146-021-00715-8

Hall R (2012) Late Jurassic-Cenozoic reconstructions of the Indonesian region and the Indian Ocean. Tectonophysics 570–571:1–41. https://doi.org/10.1016/j.tecto.2012.04.021

Hanor JS (1979) The sedimentary genesis of hydrothermal fluids. In: Barnes HL (ed) Geochemistry of hydrothermal ore deposits, 2nd edn. Wiley, New York, pp 137–172

Harbury NA, Jones ME, Audley-Charles MG, Metcalfe I, Mohamad KR (1990) Structural evolution of Mesozoic Peninsular Malaysia. J Geol Soc Lond 147:11–26. https://doi.org/10.1144/gsjgs.147.1.0011

Harris PM, Kendall CGSTC, Lerche I (1985) Carbonate cementation - a brief review. In: Schneidermann N, Harris PM (eds) Carbonate cements. SEPM, Tulsa, pp 79–95. https://doi.org/10.2110/pec.85.36.0079

Harun Z (2002) Late Mesozoic-Early tertiary faults of Peninsular Malaysia. Geol Soc Malaysia Bull 45:117–120

Hassan MHA, Aung AK, Becker RT, Abdul Rahman NA, Ng TF, Ghani AA, Shuib MK (2014) Stratigraphy and palaeoenvironmental evolution of the mid-to upper Palaeozoic succession in Northwest Peninsular Malaysia. J Asian Earth Sci 83:60–79. https://doi.org/10.1016/j.jseaes.2014.01.016

He Y, Bao ZD, Shen AJ, Shen YM, Li MH (2006) The Genetic mechanism of dolostones of the Cambrian-Lower Ordovician in Yaha-Yingmaili Region, Tarim Basin: dolomitization through deep buried hydrothermal fluid. Acta Sedimentol Sin 24:806–816 (**in Chinese with English abstract**)

Hou Y, Azmy K, Berra F, Jadoul F, Blamey NJF, Gleeson SA, Brand U (2016) Origin of the Breno and Esino dolomites in the western Southern Alps (Italy): implications for a volcanic influence. Mar Petrol Geol 69:38–52. https://doi.org/10.1016/j.marpetgeo.2015.10.010

Huang SJ, Qing H, Pei CR, Hu ZW, Wu SJ, Sun ZL (2006) Strontium concentration isotope composition and dolomitization fluids in the Feixianguan Formation of Triassic, Eastern Sichuan of China. Acta Petrol Sin 22:2123–2132 (**in Chinese with English abstract**)

Hutchison CS (1994) Gondwana and Cathaysian blocks, palaeotethys sutures and Cenozoic tectonics in Southeast Asia. Geol Rundsch 83(2):388–405. https://doi.org/10.1007/BF00210553

Jacobsen SB, Kaufman AJ (1999) The Sr, C and O isotopic evolution of Neoproterozoic seawater. Chem Geol 161(1–3):37–57. https://doi.org/10.1016/S0009-2541(99)00080-7

James NP, Jones B (2015) Origin of carbonate sedimentary rocks. Wiley, Chichester

Johannessen KC, Vander Roost J, Dahle H, Dundas SH, Pedersen RB, Thorseth IH (2017) Environmental controls on biomineralization and Fe-mound formation in a low-temperature hydrothermal system at the Jan Mayen Vent Fields. Geochim Cosmochim Acta 202:101–123. https://doi.org/10.1016/j.gca.2016.12.016

Jones CR (1970) The geology and mineral resources of the Grik Area, Upper Perak, vol 11. Geological Survey, West Malaysia, p 144

Kaczmarek SE, Sibley DF (2011) On the evolution of dolomite stoichiometry and cation order during high-temperature synthesis experiments: an alternative model for the geochemical evolution

of natural dolomites. Sediment Geol 240(1–2):30–40. https://doi.org/10.1016/j.sedgeo.2011.07.003

Kadir AA, Pierson B, Zuhar Z, Chow W (2011) Impressive slump structures in Permo-Carboniferous limestone at Sg. Siput, Perak, Malaysia. In: First EAGE South-East Asia Regional Geology Workshop-Workshop on Palaeozoic Limestones of South-East Asia and South China. https://doi.org/10.3997/2214-4609.20144016

Kamber BS, Webb GE (2001) The geochemistry of late Archaean microbial carbonate: implications for ocean chemistry and continental erosion history. Geochim Cosmochim Acta 65:2509–2525. https://doi.org/10.1016/S0016-7037(01)00613-5

Kamber BS, Greig A, Collerson KD (2005) A new estimate for the composition of weathered young upper continental crust from alluvial sediments, Queensland, Australia. Geochim Cosmochim Acta 69(4):1041–1058. https://doi.org/10.1016/j.gca.2004.08.020

Kaufman AJ, Knoll AH (1995) Neoproterozoic variations in the C-isotopic composition of seawater: stratigraphic and biogeochemical implications. Precambrian Res 73(1–4):27–49. https://doi.org/10.1016/0301-9268(94)00070-8

Kawakami T, Nakano N, Higashino F, Hokada T, Osanai Y, Yuhara M, Charusiri P, Kamikubo H, Yonemura K, Hirata T (2014) U-Pb zircon and CHIME monazite dating of granitoids and high-grade metamorphic rocks from the Eastern and Peninsular Thailand - a new report of Early Paleaozoic granite. Lithos 200–201:64–79. https://doi.org/10.1016/j.lithos.2014.04.012

Kirmaci MZ (2008) Dolomitization of the late Cretaceous-Paleocene platform carbonates, Gölköy (Ordu), eastern Pontides, NE Turkey. Sediment Geol 203(3–4):289–306. https://doi.org/10.1016/j.sedgeo.2007.12.009

Kirmaci MZ, Akdag K (2005) Origin of dolomite in the Late Cretaceous-Paleocene limestone turbidites, Eastern Pontides, Turkey. Sediment Geol 181(1–2):39–57. https://doi.org/10.1016/j.sedgeo.2005.07.003

Krähenbuhl R (1991) Magmatism, tin mineralization and tectonics of the Main Range, Malaysia Peninsula: consequences for the plate tectonic model for Southeast Asia based on Rb-Sr, K-Ar and fission track data. Geol Soc Malaysia Bull 29:1–100

Kučera J, Cempírek J, Dolníček Z, Muchez P, Prochaska W (2009) Rare earth elements and yttrium geochemistry of dolomite from post-Variscan vein-type mineralization of the NízkýJeseník and Upper Silesian Basins, Czech Republic. J Geochem Explor 103(2–3):69–79. https://doi.org/10.1016/j.gexplo.2009.08.001

Kupecz JA, Land LS (1994) Progressive recrystallization and stabilization of early-stage dolomite: lower Ordovician Ellenburger Group, West Texas. In: Purser B, Tucker M, Zenger D (eds) Dolomites: a volume in honour of Dolomieu. Blackwell, Oxford, UK, pp 255–279. https://doi.org/10.1002/9781444304077.ch15

Kupecz JA, Montanez IP, Gao G (1993) Recrystallization of dolomite with time. In: Rezak R, Lavoie DL (eds) Carbonate microfabrics. Springer, New York, pp 187–194. https://doi.org/10.1007/978-1-4684-9421-1_14

Land LS (1980) The isotopic and trace element geochemistry of dolomite: the state of the art. In: Zenger DH, Dunham JB, Ethington RL (eds) Concepts and models of dolomitization. SEPM, Tulsa, pp 87–110. https://doi.org/10.2110/pec.80.28.0087

Land LS (1985) The origin of massive dolomite. J Geol Educ 33:112–125

Land LS (1986) Environments of limestone and dolomite diagenesis: some geochemical considerations. Colo Sch Mines Quart 81:26–41

Land LS (1991) Dolomitization of the Hope Gate Formation (north Jamaica) by seawater: reassessment of mixing-zone dolomite. In: Taylor HP, Taylor O'Neil Jr JR, Kaplan IR (eds) Stable isotope chemistry: a tribute to Samuel Epstein. Geochem Soc Special Publication, London, pp 121–133

Land LS, Hoops GK (1973) Sodium in carbonate sediments and rocks: a possible index to the salinity of diagenetic solutions. J Sediment Res 43:614–617. https://doi.org/10.1306/74D7281A-2B21-11D7-8648000102C1865D

Lawrence MG, Greig A, Collerson KD, Kamber BS (2006) Rare earth element and yttrium variability in south east Queensland waterways. Aquat Geochem 12:39–72

Lee CP (2009) Palaeozoic stratigraphy. In: Hutchison CS, Tan DNK (eds) Geology of Peninsular Malaysia. University of Malaya and Geol Soc Malaysia, Kuala Lumpur, pp 55–86

Lee S, Lee D, Kim Y, Chae B, Kim W, Woo N (2003) Rare earth elements as indicators of groundwater environment changes in a fractured rock system: evidence from fracture-filling calcite. Appl Geochem 18(1):135–143. https://doi.org/10.1016/S0883-2927(02)00071-9

Li Q, Jiang Z, Hu W, You X (2015) Origin of dolomite in the Middle Triassic Zhouchongcun Formation, central lower Yangtze region, Southeast China. Carpathian J Earth Environ Sci 1:89–100

Li WP, Zheng YF, Zhao YY (2017) Geochemical evidence from marine carbonate for enhanced terrigenous input into seawater during the Ediacaran-Cambrian transition in South China. Precambrian Res 291:83–97. https://doi.org/10.1016/j.precamres.2017.01.015

Li F, Webb GE, Algeo TJ, Kershaw S, Lu C, Oehlert AM, Tan X (2019a) Modern carbonate ooids preserve ambient aqueous REE signatures. Chem Geol 509:163–177. https://doi.org/10.1016/j.chemgeo.2019.01.015

Li X, Liy Y, Wu CC, Sun R, Zheng L, Lone MA, Shen CC (2019b) Coral-inferred monsoon and biologically driven fractionation of offshore seawater rare earth elements in Beibu Gulf, northern South China Sea. Solid Earth Sciences 4(4):131–141. https://doi.org/10.1016/j.sesci.2019.09.003

Liu YG, Miah MRU, Schmitt RA (1988) Cerium, a chemical tracer for paleo-oceanic redox conditions. GeochimCosmochim Acta 52:1361–1371. https://doi.org/10.1016/0016-7037(88)90207-4

Liu X, Hardisty DS, Lyons TW, Swart PK (2019) Evaluating the fidelity of the cerium paleoredox tracer during variable carbonate diagenesis on the Great Bahamas Bank. GeochimCosmochim Acta 248:25–42. https://doi.org/10.1016/j.gca.2018.12.028

Lonne J, Al-Aasm IS (2000) Dolomitization and fluid evolution in the Middle Devonian sulphur point formation, Rainbow South Field, Alberta: petrographic and geochemical evidence. Bull Can Petrol Geol 48(3):262–283. https://doi.org/10.2113/48.3.262

Lu FH, Meyers WJ (1998) Massive dolomitization of Late Miocene carbonate platform: a case of mixed evaporate brines with meteoric water, Nijar, Spain. Sedimentology 45(2):263–277. https://doi.org/10.1046/j.1365-3091.1998.0142e.x

Machel HG (2004) Concepts and models of dolomitization: a critical reappraisal. Geol Soc Lond, Spec Publ 235:7–63. https://doi.org/10.1144/GSL.SP.2004.235.01.02

MacDonald J, John C, Girard JP (2015) Dolomitization processes in hydrocarbon reservoirs: insight from geothermometry using clumped isotopes. Procedia Earth Planet Sci 13:265–268. https://doi.org/10.1016/j.proeps.2015.07.062

MacLeod KG, Irving AJ (1996) Correlation of cerium anomalies with indicators of paleoenvironment. J Sediment Res 66(5):948–955. https://doi.org/10.1306/D426844B-2B26-11D7-8648000102C1865D

Mahboubi A, Nowrouzi Z, Al-Aasm IS, Moussavi-Harami R, Mahmudy-Gharaei MH (2016) Dolomitization of the Silurian Niur formation, tabas block, east central Iran: fluid flow and dolomite evolution. Mar Petrol Geol 77:791–805. https://doi.org/10.1016/j.marpetgeo.2016.07.023

Malone MJ, Baker PA, Burns SJ (1996) Recrystallization of dolomite: an experimental study from 50 to 200 ℃. Geochim Cosmochim

Acta 60(12):2189–2207. https://doi.org/10.1016/0016-7037(96)00062-2

Martín-Martín JD, Travé A, Gomez-Rivas E, Salas R, Sizun J, Vergés J, Corbella M, Stafford SL, Alfonso P (2015) Fault-controlled and stratabound dolostones in the late Aptian-earliest Albian Benassal formation (Maestrat Basin, E Spain): petrology and geochemistry constrains. Mar Petrol Geol 65:83–102. https://doi.org/10.1016/j.marpetgeo.2015.03.019

Mazzullo SJ (1992) Geochemical and neomorphic alteration of dolomite: a review. Carb Evap 7:21–37

Md Ali MA, Willingshofer E, Matenco L, Francois T, Daanen TP, Ng TF, Taib NI, Shuib MK (2016) Kinematics of post-orogenic extension and exhumation of the Taku Schist, NE Peninsular Malaysia. J Asian Earth Sci 127:63–75. https://doi.org/10.1016/j.jseaes.2016.06.020

Mehmandosti EA, Adabi MH (2013) Application of geochemical data as evidence of water-rock interaction in the Sarvak formation, Izeh Zone, Zagros, Iran. Procedia Earth Planet Sci 7:31–35. https://doi.org/10.1016/j.proeps.2013.03.216

Meng DD, Pubellier M, Sautter B, Beg MA (2021) Zircon U-Pb ages of the Benom complex: implications for a late Triassic uplift event in central Peninsular Malaysia. Bull Geol Soc Malaysia 72:1–13. https://doi.org/10.7186/bgsm72202101

Metcalfe I (1991) Late Palaeozoic and Mesozoic Palaeogeography of Southeast Asia. Palaeogeogr Palaeoclimatol Palaeoecol 87(1–4):211–221. https://doi.org/10.1016/0031-0182(91)90136-F

Metcalfe I (2011a) Tectonic framework and Phanerozoic evolution of Sundaland. Gondwana Res 19(1):3–21. https://doi.org/10.1016/j.gr.2010.02.016

Metcalfe I (2011b) Palaeozoic-Mesozoic history of SE Asia. Geol Soc Lond, Spec Publ 355:7–35. https://doi.org/10.1144/SP355.2

Metcalfe I (2013) Tectonic evolution of the Malay Peninsula. J Asian Earth Sci 76:195–213. https://doi.org/10.1016/j.jseaes.2012.12.011

Michard A (1989) Rare earth element systematics in hydrothermal fluids. Geochim Cosmochim Acta 53(3):745–750. https://doi.org/10.1016/0016-7037(89)90017-3

Mohammad Zahir NA, Beg MA, Kadir AA (2020) Hydrothermal dolomitization on Devonian to carboniferous carbonates in Kinta Valley, Perak, Malaysia: a petrographic study. Indones J Geosci 7(1):25–39. https://doi.org/10.17014/ijog.7.1.25-39

Nagarajan R, Madhavaraju J, Armstrong-Altrin JS, Nagendra R (2011) Geochemistry of Neoproterozoic limestones of the Shahabad formation, Bhima Basin, Karnataka, Southern India. Geosci J 15(1):9–25. https://doi.org/10.1007/s12303-011-0005-0

Nagarajan R, Armstrong-Altrin JS, Sial AN, Nagendra R, Ellam RM (2013) Carbon, oxygen, and strontium isotope geochemistry of the proterozoic carbonate rocks, Bhima Basin, South India: implication for diagenesis. Carpathian J Earth Environ Sci 8(2):25–38

Navarro-Ciurana D, Cardellach E, Galindo C, Fuenlabrada JM, Griera A, Gómez-Gras D, Vindel E, Corbella M (2017) REE and Sm-Nd clues of high-temperature fluid-rock interaction in the Riópar dolomitization (SE Spain). Procedia Earth Planetary Sci 17:448–451. https://doi.org/10.1016/j.proeps.2016.12.113

Ng SWP, Chung SL, Robb LJ, Searle MP, Ghani AA, Whitehouse MJ, Oliver GJH, Sone M, Gardiner NJ, Roselee MH (2015a) Petrogenesis of Malaysian granitoids in the Southeast Asian tin belt: Part 1. Geochemical and Sr-Nd isotopic characteristics. Bull Geol Soc Am 127(9–10):1209–1237. https://doi.org/10.1130/B31213.1

Ng SWP, Whitehouse MJ, Searle MP, Robb LJ, Ghani AA, Chung SL, Oliver GJH, Sone M, Gardiner NJ, Roselee MH (2015b) Petrogenesis of Malaysian granitoids in the Southeast Asian tin belt: Part 2. U-Pb zircon geochronology and tectonic model. Bull Geol Soc Am 127(9–10):1238–1258. https://doi.org/10.1130/B31214.1

Nguyen A, Zhao J, Feng Y, Hu W, Yu K, Gasparon M, Pham T, Clark T (2013) Impact of recent coastal development and human activities on Nha Trang Bay, Vietnam: evidence from a *Porites lutea* geochemical record. Coral Reefs 32(1):181–193. https://doi.org/10.1007/s00338-012-0962-4

Nothdurft LD, Webb GE, Kamber BS (2004) Rare earth element geochemistry of Late Devonian reefal carbonates, Canning Basin, Western Australia: confirmation of a seawater proxy in ancient limestones. Geochim Cosmochim Acta 68(2):263–283. https://doi.org/10.1016/S0016-7037(03)00422-8

Nozaki Y, Zhang J, Amakawa H (1997) The fractionation between Y and Ho in the marine environment. Earth Planet Sci Lett 148(1–2):329–340. https://doi.org/10.1016/S0012-821X(97)00034-4

Nozaki Y, Lerche D, Alibo DS, Snidvongs A (2000) The estuarine geochemistry of rare earth elements and indium in the Chao Phraya River, Thailand. Geochim Cosmochim Acta 64(23):3983–3994. https://doi.org/10.1016/S0016-7037(00)00473-7

Palmer MR (1985) Rare earth elements in foraminifera tests. Earth Planet Sci Lett 73(2–4):285–298. https://doi.org/10.1016/0012-821X(85)90077-9

Picard P, Lécuyer C, Barrat J, Garcia J, Dromart G, Sheppard SMF (2002) Rare earth element contents of Jurassic fish and reptile teeth and their potential relation to seawater composition (Anglo–Paris Basin, France and England). Chem Geol 186(1–2):1–16. https://doi.org/10.1016/S0009-2541(01)00424-7

Pierson BJ (1981) The control of cathodoluminescence in dolomite by iron and manganese. Sedimentology 28(5):601–610. https://doi.org/10.1111/j.1365-3091.1981.tb01924.x

Piepgras DJ, Jacobsen SB (1992) The behaviour of rare earth elements in seawater: precise determination of ferromanganese crusts. Geochim Cosmochim Acta 56:1851–1862. https://doi.org/10.1016/0016-7037(92)90315-A

Piper DZ (1974a) Rare earth elements in the sedimentary cycle, a summary. Chem Geol 14(4):285–304. https://doi.org/10.1016/0009-2541(74)90066-7

Piper DZ (1974b) Rare earth elements in ferromanganese nodules and other marine phases. Geochim Cosmochim Acta 38(7):1007–1022. https://doi.org/10.1016/0016-7037(74)90002-7

Planavsky N, Bekker A, Rouxel OJ, Kamber B, Hofmann A, Knudsen A, Lyons TW (2010) Rare earth element and yttrium compositions of Archean and Paleoproterozoic Fe formations revisited: new perspectives on the significance and mechanisms of deposition. Geochim Cosmochim Acta 74(22):6387–6405. https://doi.org/10.1016/j.gca.2010.07.021

Purser B, Brown A, Aissaoui DM (1994) Nature, origins and evolution of porosity in dolomite. In: Purser B, Tucker M, Zenger D (eds) Dolomites: a volume in honour of Dolomieu. Wiley, Oxford, UK, pp 283–308

Qing H, Mountjoy EW (1989) Multistage dolomitization in rainbow buildups, Middle Devonian Keg River formation, Alberta, Canada. J Sediment Res 59(1):114–126. https://doi.org/10.1306/212F8F30-2B24-11D7-8648000102C1865D

Qing H, Mountjoy EW (1994) Formation of coarsely crystalline, hydrothermal dolomite reservoirs in the Presqu'ile Barrier, Western Canada Sedimentary Basin. AAPG Bull 78(1):55–77. https://doi.org/10.1306/BDFF9014-1718-11D7-8645000102C1865D

Rahimi A, Adabi MH, Aghanabati A, Majidifard MR, Jamali AM (2016) Dolomitization mechanism based on petrography and geochemistry in the Shotori formation (Middle Triassic), Central Iran. Open J Geol 6(9):1149–1168. https://doi.org/10.4236/ojg.2016.69085

Ramkumar M (2007) Dolomitic limestone in the Kallankurichchi formation (Lower Maastrichtian) Ariyalur Group, South India. J Earth Sci 1(1):7–21

Ramkumar M (2008) Carbonate diagenesis in the Kallankurichchi formation, Ariyalur Group, south India and its implications on petroleum prospects. J Geol Soc Ind 71:407–418

Ramkumar M, Stüben D, Berner Z (2006) Elemental interrelationships and depositional controls of Barremian-Danian strata of the Cauvery Basin, South India: Implications on scales of chemostratigraphic modelling. Ind J Geochem 21:341–367

Ramkumar M, Alberti M, Fürsich FT, Pandey DK (2013) Depositional and diagenetic environments of the Dhosa Oolite Member (Oxfordian), Kachchh Basin, India, based on petrographic data: Implications on the origin and occurrence of ooids and their correlation with global oolite peak. In: Ramkumar M (ed) On a sustainable future of the earth's natural resources. Springer, Heidelberg, pp 179–230. https://doi.org/10.1007/978-3-642-32917-3_11

Ramkumar M, Alberti M, Fürsich FT (2014) Interpretation of Palaeoclimate, relative sealevel and scale of stratigraphic correlation through spatio-temporal variations in depositional and diagenetic environments: a case study. In: Sinha S (ed) Advances in petroleum engineering. Studium Press LLC, USA, pp 284–307

Ramkumar M, Siddiqui NA, Mathew M, Sautter B, Xin Hui P, Nagarajan R, Breitfeld HT, Santosh M, Menier D, Poppelreiter M (2019) Structural controls on polyphase hydrothermal dolomitization in the Kinta Valley, Malaysia: paragenesis and regional tectonomagmatism. J Asian Earth Sci 174:364–380. https://doi.org/10.1016/j.jseaes.2019.02.004

Rastall RH (1927) The limestone of the Kinta Valley, Federated Malay States. Geol Mag 64:410–342

Reynard B, Lécuyer C, Grandjean P (1999) Crystal-chemical controls on rare-earth element concentrations in fossil biogenic apatites and implications for paleoenvironmental reconstructions. Chem Geol 155(3–4):233–241. https://doi.org/10.1016/S0009-2541(98)00169-7

Ronchi P, Masetti D, Tassan S, Camocino D (2012a) Hydrothermal dolomitization in platform and basin carbonate successions during thrusting: a hydrocarbon reservoir analogue (Mesozoic of Venetian Southern Alps, Italy). Mar Petrol Geol 29(1):68–89. https://doi.org/10.1016/j.marpetgeo.2011.09.004

Ronchi P, Consonni A, Borromeo O, Battistelli A, Geloni C (2012b) Reactive transport modelling applied to the prediction of the dolomitization distribution in carbonate hydrocarbon reservoirs. First Break 30(10):57–65. https://doi.org/10.3997/1365-2397.2012015

Saleem M, Sajjad SW, Khan EU, Naseem AA, Bangash AA, Rafique A, Hussain S, Ullah H, Khan S, Ahmad W (2022) Classification of the dolomites of Cretaceous Kawagarh formation in Hazara Basin North-west Himalayas Pakistan: evidence from field investigation, petrographic analysis and isotopic studies. Carbonates Evaporites. https://doi.org/10.1007/s13146-022-00760-x

Sass E, Bein A (1988) Dolomites and salinity: a comparative geochemical study. In: Shukla V, Baker PA (eds) Sedimentology and geochemistry of dolostones. SEPM, Tulsa, pp 223–233

Sautter B, Pubellier M, Jousselin P, Dattilo P, Kerdraon Y, Meng CC, Menier D (2017) Late paleogene rifting along the Malay Peninsula thickened crust. Tectonophysics 710:205–224. https://doi.org/10.1016/j.tecto.2016.11.035

Sautter B, Pubellier M, Králiková Schlögl S, Matenco L, Andriessen P, Mathew M (2019) Exhumation of west Sundaland: a record of the path of India? Earth Sci Revs 198:102933. https://doi.org/10.1016/j.earscirev.2019.102933

Schwinn G, Markl G (2005) REE systematics in hydrothermal fluorite. Chem Geol 216(3–4):225–248. https://doi.org/10.1016/j.chemgeo.2004.11.012

Searle MP, Whitehouse MJ, Robb LJ, Ghani AA, Hutchison CS, Sone M, Ng SWP, Roselee MH, Chung S, Oliver GJH (2012) Tectonic evolution of the Sibumasu-Indochina terrane collision zone in Thailand and Malaysia: constraints from new U-Pb zircon chronology of SE Asian tin granitoids. J Geol Soc Lond 169(4):489–500. https://doi.org/10.1144/0016-76492011-107

Shanmugam G, Benedict GL (1983) Manganese distribution in the carbonate fraction of shallow and deep marine lithofacies, Middle Ordovician, Eastern Tennessee. Sediment Geol 35(3):159–175. https://doi.org/10.1016/0037-0738(83)90036-2

Shields G, Stille P (2001) Diagenetic constraints on the use of cerium anomalies as palaeoseawater redox proxies: an isotopic and REE study of Cambrian phosphorites. Chem Geol 175(1–2):29–48. https://doi.org/10.1016/S0009-2541(00)00362-4

Shields GA, Webb GE (2004) Has the REE composition of seawater changed over geological time? Chem Geol 204(1–2):103–107. https://doi.org/10.1016/j.chemgeo.2003.09.010

Shuib MK (2009) Major faults. In: Hutchison CS, Tan DNK (eds) Geology of Peninsular Malaysia. University of Malaya and Geological Society of Malaysia, Kuala Lumpur, pp 249–269

Sibley DF, Gregg JM (1987) Classification of dolomite rock texture. J Sediment Res 57(6):967–975. https://doi.org/10.1306/212F8CBA-2B24-11D7-8648000102C1865D

Sibley DF, Nordeng SH, Borkowski ML (1994) Dolomitization kinetics in hydrothermal bombs and natural settings. J Sediment Res 64(3a):630–637. https://doi.org/10.1306/D4267E29-2B26-11D7-8648000102C1865D

Slack J, Grenne T, Bekker A, Rouxel O, Lindberg P (2007) Suboxic deep seawater in the late Paleoproterozoic: evidence from hematitic chert and iron formation related to seafloor-hydrothermal sulfide deposits, central Arizona, USA. Earth Planet Sci Lett 255:243–256. https://doi.org/10.1016/j.epsl.2006.12.018

Smrzka D, Zwicker J, Bach W, Feng D, Himmler T, Chen D, Peckmann J (2019) The behavior of trace elements in seawater, sedimentary pore water, and their incorporation into carbonate minerals: a review. Facies 65:41. https://doi.org/10.1007/s10347-019-0581-4

Sperber CM, Wilkinson BH, Peacor DR (1984) Rock composition, dolomite stoichiometry, and water/rock interactions in dolomite carbonate rocks. J Geol 92:609–622. https://doi.org/10.1086/628901

Srivastava VK, Singh BP (2019) Depositional environments and sources for the middle Eocene Fulra limestone formation, Kachchh Basin, western India: evidences from facies analysis, mineralogy, and geochemistry. Geol J 54:62–82. https://doi.org/10.1002/gj.3154

Stanley SM (2008) Effects of global seawater chemistry on biomineralization: past, present, and future. Chem Rev 108(11):4483–4498. https://doi.org/10.1021/cr800233u

Subramanyam KSV, Balaram V, Manikyamba RP, Krishna AK, Sawant SS, Narshimha C (2020) Geochemistry of marine carbonates from hole 1394, off the coast of Montserrat, IODP expedition-340; implications on provenance, paleoenvironment and lesser Antilles Arc Migration. In: Pandey D, Ravichandran M, Nair N (eds) Dynamics of the earth system: evolution, processes and interactions. Society of earth scientists series. Springer, Cham, pp 101–140. https://doi.org/10.1007/978-3-030-40659-2_6

Sun SQ (1995) Dolomite reservoirs: porosity evolution and reservoir characteristics. AAPG Bull 79(2):186–204

Taylor SR, McLennan SM (1985) The continental crust: its composition and evolution. Blackwell, Oxford, p 312

Tostevin R (2021) Cerium anomalies and paleoredox (elements in geochemical tracers in earth system science). Cambridge University Press, Cambridge, p 75. https://doi.org/10.1017/9781108847223

Tostevin R, Shields GA, Tarbuck GM, He T, Clarkson MO, Wood RA (2016) Effective use of cerium anomalies as a redox proxy in carbonate-dominated marine settings. Chem Geol 438:146–162. https://doi.org/10.1016/j.chemgeo.2016.06.027

Toyoda K, Nakamura Y, Masuda A (1990) Rare earth elements of Pacific pelagic sediments. Geochim Cosmochim Acta 54(4):1093–1103. https://doi.org/10.1016/0016-7037(90)90441-M

Tucker ME, Wright VP (1990) Dolomites and dolomitization models. In: Tucker ME, Wright VP (eds) Carbonate sedimentology. Blackwell, Oxford, pp 365–400

Vahrenkamp VC, Swart PK (1990) New distribution coefficient for the incorporation of strontium into dolomite and its implications for the formation of ancient dolomites. Geology 18(5):387–391. https://doi.org/10.1130/0091-7613(1990)018%3C0387:NDCFTI%3E2.3.CO;2

Vandeginste V, John CM, Flierdt T, Cosgrove JW (2013) Linking process, dimension, texture and geochemistry in dolomite geobodies: a case study from Wadi Mistal (northern Oman). AAPG Bull 97(7):1181–1207. https://doi.org/10.1306/11011212076

Veizer J (1978) Secular variations in the composition of sedimentary carbonate rocks, II. Fe, Mn, Ca, Mg, Si and minor constituents. Precambrian Res 6(3–4):381–413. https://doi.org/10.1016/0301-9268(78)90024-4

Veizer J (1983a) Trace elements and isotopes in sedimentary carbonates. Rev Mineral Geochem 11:265–300

Veizer J (1983b) Chemical diagenesis of carbonates: Theory and application of trace element technique. In: Arthur MA, Anderson TF, Kaplan IR, Veizer J, Land LS (eds) Stable isotopes in sedimentary geology. SEPM, Tulsa, pp III1–III100

Veizer J, Clayton RN, Hinton RW, Von Brunn V, Mason TR, Buck SG, Hoefs J (1990) Geochemistry of Precambrian carbonates: III. Shelf seas and non-marine environments of the Archean. Geochim Cosmochim Acta 54:2717–2729. https://doi.org/10.1016/0016-7037(90)90007-8

Veizer J, Lemieux J, Jones B, Gibling MR, Savelle J (1977) Sodium: paleosalinity indicator in ancient carbonate rocks. Geology 5(3):177–179. https://doi.org/10.1130/0091-7613(1977)5%3C177:SPIIAC%3E2.0.CO;2

Wakita K, Metcalfe I (2005) Ocean plate stratigraphy in East and Southeast Asia. J Asian Earth Sci 24(6):679–702. https://doi.org/10.1016/j.jseaes.2004.04.004

Wang XL, Jin ZJ, Hu WX, Zhang JT, Qian YX, Zhu JQ, Li Q (2009) Using in situ REE analysis to study the origin and diagenesis of dolomite of Lower Paleaozoic, Tarim Basin. Sci China Ser D Earth Sci 52(5):681–693. https://doi.org/10.1007/s11430-009-0057-4

Wang L, Hu W, Wang X, Cao J, Chen Q (2014) Seawater normalized REE patterns of dolomites in Geshan and Panlongdong sections, China: Implications for tracing dolomitization and diagenetic fluids. Mar Petrol Geol 56:63–73. https://doi.org/10.1016/j.marpetgeo.2014.02.018

Warren J (2000) Dolomite: occurrence, evolution and economically important associations. Earth-Sci Rev 52(1–3):1–81. https://doi.org/10.1016/S0012-8252(00)00022-2

Webb GE, Kamber BS (2000) Rare earth elements in Holocene reefal microbialites: a new shallow seawater proxy. Geochim Cosmochim Acta 64(9):1557–1565. https://doi.org/10.1016/S0016-7037(99)00400-7

Wilson MEJ, Evans MJ, Oxtoby NH, Nas DS, Donnelly T, Thirlwall M (2007) Reservoir quality, textural evolution, and origin of fault-associated dolomites. AAPG Bull 91(9):1247–1272. https://doi.org/10.1306/05070706052

Xin Hui P, Ramkumar M, Nagarajan R, Mathew MJ, Ng TF (2021) Episodic dolomitization of Paleaozoic limestones in the Kinta Valley, Malaysia: implications on porosity evolution and reservoir properties. Energy Geosci 2(4):298–307. https://doi.org/10.1016/j.engeos.2020.11.003

Yamamoto K, Itoh N, Matsumoto T, Tanaka T, Adachi M (2004) Geochemistry of Precambrian carbonate intercalated in pillows and its host basalt: implications for the REE composition of circa 34 Ga seawater. Precambrian Res 135(4):331–344. https://doi.org/10.1016/j.precamres.2004.09.006

Zenger DH, Dunham JB, Ethington RL (1980) Concepts and models of dolomitization. SEPM, Tulsa, p 320. https://doi.org/10.2110/pec.80.28

Zhang J, Nozaki Y (1998) Behavior of rare earth elements in seawater at the ocean margin: a study along the slopes of the Sagami and Nankai troughs near Japan. Geochim Cosmochim Acta 62(8):1307–1317. https://doi.org/10.1016/S0016-7037(98)00073-8

Zhang J, Hu W, Qian Y, Wang X, Cao J, Zhu J, Li Q, Xie X (2009) Formation of saddle dolomites in Upper Cambrian carbonates, western Tarim Basin (northwest China): implications for fault-related fluid flow. Mar Petrol Geol 26:1428–1440. https://doi.org/10.1016/j.marpetgeo.2009.04.004

Zhang W, Guan P, Jian X, Feng F, Zou C (2014) In situ geochemistry of Lower Paleaozoic dolomites in the northwestern Tarim basin: Implications for the nature, origin, and evolution of diagenetic fluids. Geochem Geophys Geosyst 15:2744–2764. https://doi.org/10.1002/2013GC005194

Zhao H, Jones B (2012) Genesis of fabric-destructive dolostones: a case study of the Brac formation (Oligocene), Cayman Brac, British West Indies. Sediment Geol 267–268:36–54. https://doi.org/10.1016/j.sedgeo.2012.05.007

Zhao H, Jones B (2013) Distribution and interpretation of rare earth elements and yttrium in Cenozoic dolostones and limestones on Cayman Brac, British West Indies. Sediment Geol 284–285:26–38. https://doi.org/10.1016/j.sedgeo.2012.10.009

Zhao MY, Zheng YF (2014) Marine carbonate records of terrigenous input into Paleotethyan seawater: geochemical constraints from carboniferous limestones. Geochim Cosmochim Acta 141:508–531. https://doi.org/10.1016/j.gca.2014.07.001

Zhao Y, Zhao M, Li SZ (2018) Evidences of hydrothermal fluids recorded in microfacies of the Ediacaran cap dolostone: geochemical implications in South China. Precambrian Res 306:1–21. https://doi.org/10.1016/j.precamres.2017.12.028

Zhong S, Mucci A (1995) Partitioning of rare earth elements between calcite and seawater solutions at 25 ℃ and 1 atm, and high dissolved REE concentrations. Geochim Cosmochim Acta 59(3):443–453. https://doi.org/10.1016/0016-7037(94)00381-U

Publisher's Note Springer Nature remains neutral with regard to jurisdictional claims in published maps and institutional affiliations.

Authors and Affiliations

P. Xin Hui[1] · R. Nagarajan[2,3] · Mu. Ramkumar[4,5] · T. F. Ng[6] · Nur I. Taib[6] · M. J. Mathew[7] · B. Sautter[8] · N. A. Siddiqui[1] · M. C. Poppelreiter[5]

P. Xin Hui
poonxh@gmail.com

Mu. Ramkumar
muramkumar@yahoo.co.in

T. F. Ng
ntf@um.edu.my

Nur I. Taib
iskandartaib@um.edu.my

M. J. Mathew
manoj_mathew7@yahoo.com

B. Sautter
Benjamin_sautter@hotmail.fr

N. A. Siddiqui
numairpng@gmail.com

M. C. Poppelreiter
M.Poppelreiter@SHELL.com

[1] Department of Geoscience, Universiti Teknologi PETRONAS, Seri Iskandar, Malaysia

[2] Department of Applied Sciences (Applied Geology), Curtin University Malaysia, 98009 Miri, Sarawak, Malaysia

[3] Curtin Malaysia Research Institute, Curtin University, 98009 Miri, Sarawak, Malaysia

[4] Department of Geology, Periyar University, Salem 636011, India

[5] South East Asia Carbonate Research Laboratory (SEACaRL), Universiti Teknologi PETRONAS, Seri Iskandar, Malaysia

[6] Department of Geology, University of Malaya, Kuala Lumpur, Malaysia

[7] Laboratoire Géoscience Océan, UMR CNRS/UBO/UBS 6538, IUEM, Université de Brest, 29280 Plouzané, France

[8] Commission for the Geological Map of the World (CGMW), 77 Rue Claude Bernard, 75005 Paris, France